Development/Plasticity/Repair

Slow Muscle Precursors Lay Down a Collagen XV Matrix Fingerprint to Guide Motor Axon Navigation

Emilie Guillon, Sandrine Bretaud, and Florence Ruggiero
Institut de Génomique Fonctionnelle de Lyon, ENS de Lyon, UMR CNRS 5242, Université Lyon 1, 69364 Lyon cedex 07, France

The extracellular matrix (ECM) provides local positional information to guide motoneuron axons toward their muscle target. Collagen XV is a basement membrane component mainly expressed in skeletal muscle. We have identified two zebrafish paralogs of the human *COL15A1* gene, *col15a1a* and *col15a1b*, which display distinct expression patterns. Here we show that *col15a1b* is expressed and deposited in the motor path ECM by slow muscle precursors also called adaxial cells. We further demonstrate that collagen XV-B deposition is both temporally and spatially regulated before motor axon extension from the spinal cord in such a way that it remains in this region after the adaxial cells have migrated toward the periphery of the myotome. Loss- and gain-of-function experiments in zebrafish embryos demonstrate that *col15a1b* expression and subsequent collagen XV-B deposition and organization in the motor path ECM depend on a previously undescribed two-step mechanism involving Hedgehog/Gli and *unplugged*/MuSK signaling pathways. *In silico* analysis predicts a putative Gli binding site in the *col15a1b* proximal promoter. Using *col15a1b* promoter-reporter constructs, we demonstrate that *col15a1b* participates in the slow muscle genetic program as a direct target of Hedgehog/Gli signaling. Loss and gain of *col15a1b* function provoke pathfinding errors in primary and secondary motoneuron axons both at and beyond the choice point where axon pathway selection takes place. These defects result in muscle atrophy and compromised swimming behavior, a phenotype partially rescued by injection of a *smyhc1:col15a1b* construct. These reveal an unexpected and novel role for collagen XV in motor axon pathfinding and neuromuscular development.

Key words: collagen; extracellular matrix; motor axon pathfinding; signaling pathway; slow muscle precursors; zebrafish

Significance Statement

In addition to the archetypal axon guidance cues, the extracellular matrix provides local information that guides motor axons from the spinal cord to their muscle targets. Many of the proteins involved are unknown. Using the zebrafish model, we identified an unexpected role of the extracellular matrix collagen XV in motor axon pathfinding. We show that the synthesis of collagen XV-B by slow muscle precursors and its deposition in the common motor path are dependent on a novel two-step mechanism that determines axon decisions at a choice point during motor axonogenesis. Zebrafish and humans use common molecular cues and regulatory mechanisms for the neuromuscular system development. And as such, our study reveals *COL15A1* as a candidate gene for orphan neuromuscular disorders.

Introduction

From spinal cord exit, motor axons are guided by attractive and repulsive cues along a stereotyped path and navigate with remarkable precision to their muscle target. Zebrafish has been particularly instrumental in identifying specialized cells and extracellular environments critical for motor axon pathfinding (Beattie, 2000). Each somitic hemisegment is innervated by three primary motoneurons (pMNs): caudal (CaP), middle (MiP), and rostral (RoP). Their axons follow a common trajectory until they reach the horizontal myoseptum, an intermediate target also known as a choice point where axons diverge to innervate the dorsal (MiP) and ventral (CaP) myotome or the horizontal myoseptum itself (RoP). Thirty secondary motoneuron axons later innervate the myotome following the path pioneered by pMNs

Received July 28, 2015; revised Dec. 27, 2015; accepted Jan. 18, 2016.

Author contributions: E.G., S.B., and F.R. designed research; E.G. and S.B. performed research; S.B. and F.R. contributed unpublished reagents/analytic tools; E.G., S.B., and F.R. analyzed data; E.G. and F.R. wrote the paper.

This work was supported by the CNRS, ENS-Lyon, University of Lyon, and Agence Nationale de la Recherche Grant 10BLAN121901. E.G. received a Ministère de l'Enseignement Supérieur et de la Recherche fellowship. We thank Andreas Faissner for C-6-S antibodies; Estelle Hirsinger for the *eng2a* probe; Stone Elworthy and Fredericus van Eeden for *dnPKA*, *Shh*, and *smyhc1* constructs and *ptch1/ptch2* mutant embryos; Michael Granato for *unplugged/MuSK* embryos; Magali Naville (Institut de Génomique Fonctionnelle de Lyon, Lyon, France) for bioinformatic analysis; Laure Bernard and Robert Renard (Plateau de Recherche Expérimentale de Criblage In vivo; PRECI) for fish care and the PLATIM (SFR Lyon-Gerland Biosciences, France); Marilyne Malbouyres and Elisabeth Vaganay for expert technical assistance; Jamilé Hazan for sharing protocols and advice; and Dominique Le Guellec for his continuing interest in the study.

The authors declare no competing financial interests.

Correspondence should be addressed to Dr. Florence Ruggiero, Institut de Génomique Fonctionnelle de Lyon, UMR CNRS 5242, ENS de Lyon, 46, Allée d'Italie, F-69364 Lyon Cedex 07, France; E-mail: florence.ruggiero@ens-lyon.fr.

DOI:10.1523/JNEUROSCI.2847-15.2016

 0270-6474/16/362663-14$15.00/0

and form the CaP-, MiP-, and RoP-like nerves that innervate the corresponding muscle territories (Beattie, 2000).

Motor innervation patterning in zebrafish is not cell-autonomous, and the myotome provides positional information to guide primary and secondary motoneuron axons along appropriate paths (Eisen and Pike, 1991; Beattie, 2000). Slow muscle precursors (adaxial cells) and muscle pioneers (MPs), a subset of Engrailed-expressing slow muscle cells, both play a critical role in motor axonogenesis (Melançon et al., 1997; Zhang and Granato, 2000). Adaxial cells, which are located adjacent to the notochord before somitogenesis, represent an important source of various extracellular matrix (ECM) components of the motor path. As such, the glycoprotein tenascin-C (Schweitzer et al., 2005) and chondroitin sulfate proteoglycans (CSPGs) (Bernhardt and Schachner, 2000; Zhang et al., 2004), both expressed by adaxial cells, have been recognized as important short-range guidance cues for axon outgrowth.

The role of collagens in axon growth and more generally in nerve development has been recently recognized (Fox, 2008). As such, the heparan sulfate proteoglycan collagen XVIII is expressed by adaxial cells (Haftek et al., 2003), and its knockdown provokes defects during early motor outgrowth (Schneider and Granato, 2006). Lack of myotomal LH3 glycosyltransferase activity in the *diwanka/lh3* mutant was suggested to be responsible for a motoneuron guidance defect through improper glycosylation of collagen XVIII (Schneider and Granato, 2006). Recently, analysis of the *stumpy/col19a1* mutant revealed that collagen XIX also plays a crucial role in motor axon guidance at intermediate targets (Hilario et al., 2010). Collagen XV shares structural similarities with collagen XVIII as they both belong to the multiplexin (multiple triple helix interruptions) subset of the collagen superfamily (Ricard-Blum and Ruggiero, 2005). Both these collagen/proteoglycan hybrids carry glycosaminoglycan chains. Contrary to collagen XVIII, collagen XV principally carries chondroitin sulfate (CS) chains (Li et al., 2000). In mice, collagen XV is mainly expressed in cardiac and skeletal muscle, and *Col15a1*$^{-/-}$ mice display mild skeletal myopathy (Eklund et al., 2001) but also defective myelination of peripheral nerves (Rasi et al., 2010).

We recently identified two paralogs of the human *COL15A1* gene in the zebrafish genome, named *col15a1a* and *col15a1b*. Both genes are expressed in the developing trunk but display distinct spatiotemporal expression patterns; whereas *col15a1a* transcripts are restricted to notochord cells (Pagnon-Minot et al., 2008), *col15a1b* is expressed in adaxial cells (Bretaud et al., 2011). Morpholino knockdown of *col15a1a* causes notable disorganization of the notochord basement membrane, resulting in improper Hedgehog (Hh) factor diffusion and subsequent defects in muscle differentiation (Pagnon-Minot et al., 2008). Here we investigate the function of the second paralog *col15a1b* in developing zebrafish. We demonstrate that zebrafish collagen XV-B (COLXV-B) is a component of the specialized motor path extracellular matrix expressed by adaxial cells upon activation of Hh and *unplugged*/MuSK signaling, which functions as a motor axon pathfinder.

Materials and Methods

Fish maintenance. AB/TU wild-type maintenance and embryo collection were performed at the zebrafish PRECI facility (Plateau de Recherche Expérimentale de Criblage In vivo, UMS CNRS 3444 Lyon Biosciences, Gerland) in compliance with French government guidelines. Embryos obtained from natural spawning were raised following standard conditions. To prevent pigmentation, 24 hpf embryos used for experiments were treated with 0.21 mM phenylthiourea (Sigma). Developmental stages are given in hours post-fertilization (hpf) and days post-fertilization (dpf) at 28.5°C according to morphological criteria (Kimmel et al., 1995). Fish were of indeterminate sex at the stages used for our experiments (1–3 dpf).

Transgenic and mutant strains. A batch of 18 hpf fixed embryos derived from a heterozygous incross of *unplugged*^{tbb72} mutants (Zhang et al., 2004) that were outcrossed with the HB9-GFP transgenic line were kindly provided by Michael Granato (University of Pennsylvania, Philadelphia). For genotyping, genomic DNA was grossly extracted by 10 min incubation at 95°C in 50 mM NaOH, followed by pH adjustment with 1 M Tris-HCl, pH 8 (1:10 final dilution). PCR on 2 μl genomic DNA was performed at an annealing temperature of 62°C with 5′-TGGCTTTCAACACATCACTCTCC-3′ (BB72GTF1) and 5′-GGTCCGCTGTCATCACATTCC-3′ (BB72GTR1) primers to amplify the *tbb72* allele. Mutant amplicons were then identified by enzymatic digestion of purified PCR products with AflII (Biolabs) and confirmed by DNA sequencing (GATC). Sixteen of 61 embryos processed for *in situ* hybridization and 55 for imaging were genotyped. Fixed embryos derived from an incross of heterozygous *lep(ptch1)*^{tj222} and *ptch2*^{hu1602} mutants were provided by Fredericus Van Eeden (University of Sheffield, Sheffield, United Kingdom). They were genotyped after immunostaining as described above using the following primers and annealing temperatures for PCR: 5-CACATTAAGATGGAAACCTG-3′ (Lptch1) and 5′-TATCGAGC CTTTATTTAGCC-3′ (Rptch1) and 53°C for *ptch1*; 5′-GTTGCTCTATCT GTGGCTGC-3′ (Lptch2) and 5′-GTTGGATCGGGTCTCTGTGA-3′ (Rptch2) and 59°C for *ptch2*. PCR products were then sequenced using the forward primers (GATC).

The *col15a1b* mutant strain (*col15a1b*^{sa12573} allele) was obtained from the European Zebrafish Resource Center (Eggenstein-Leopoldshafen, Germany). The *col15a1b*^{sa12573} mutant line carries a nonsense mutation (G/T) in exon 30 that results in a premature stop and protein truncation in the region encoding the COL3 domain (see Fig. 8*F*). Mutants were genotyped using the following primers: 5′-GATGCAAGTGGTCCCTCTGT-3′ (Lcol15a1b^{sa12573}) and 5′-GCGTTTTGCAGTGTGGTCTA-3′ (Rcol15a1b^{sa12573}). Embryos obtained from an incross of *col15a1b*$^{+/-}$ heterozygote fish were processed for immunofluorescence at 27 hpf. Genomic DNA was extracted from each embryo after imaging, and genotyping was either performed by sequencing PCR products as mentioned above or directly by PCR using the Rcol15a1b^{sa12573} primer and two forward primers containing the mutation at the 3′ end (in bold): 5′-GTCCACCAGGTCCACC **TT**-3′ (Lcol15a1b-mut) or the wild-type sequence 5′-GTCCACCAGGT CCACCTG-3′ (Lcol15a1b-wt).

Zebrafish col15a1b cloning and recombinant production of COLXV-B. To clone the full-length coding sequence of *col15a1b* (accession number LK391962), RT-PCR was performed on 2 dpf embryos. The following primers 5′-CGCGGATCCGCCACCATGAAATTTCGCCTCCTGTC-3′ (forward) and 5′-GCCTAGACTAGTTCCTTCCAGGGTGCT-3′ (reverse) containing, respectively, the sequences for the BamHI and XbaI restriction sites at the 5′ end, were used for amplification, allowing direct cloning into the pCS2+ expression vector. For COLXV-B rich supernatant production, HEK-293 EBNA cells cultured in DMEM (supplemented with 10% FBS and 50 μg/ml gentamycin) were transfected with the pCS2+-*col15a1b* construct using the calcium phosphate transfection kit (Invitrogen), according to the manufacturer's instructions. The following day, routine medium was replaced with FBS-free medium supplemented with 50 μg/ml ascorbic acid. Media were then collected 24 h later and stored at −80°C until use.

Production and purification of antibodies against zebrafish COLXV-B. Polyclonal antibodies specifically recognizing zebrafish COLXV-B were raised in rabbits by immunization with the synthetic peptide: ARREETFGQT-NNKEKT, corresponding to the noncollagenous domain NC10 255–270 sequence (see Fig. 1*N*). Specific antibodies to COLXV-B (anti-COLXV-B) were then purified by antigen affinity chromatography. Peptide synthesis, antibody production, and purification were provided by Covalab.

Western blot analysis. For Western blot analysis of COLXV-B produced in HEK-293 EBNA cells, 1 ml of culture supernatant was classically precipitated with 10% trichloroacetic acid, and pellets were resuspended in Laemmli buffer 1× (62.5 mM Tris, pH 6.8, 1% SDS, 5% glycerol, 0.1% bromophenol blue, 10 mM DTT). Proteins were separated by SDS-PAGE and transferred to PVDF membranes. Western blot analysis was then performed with affinity-

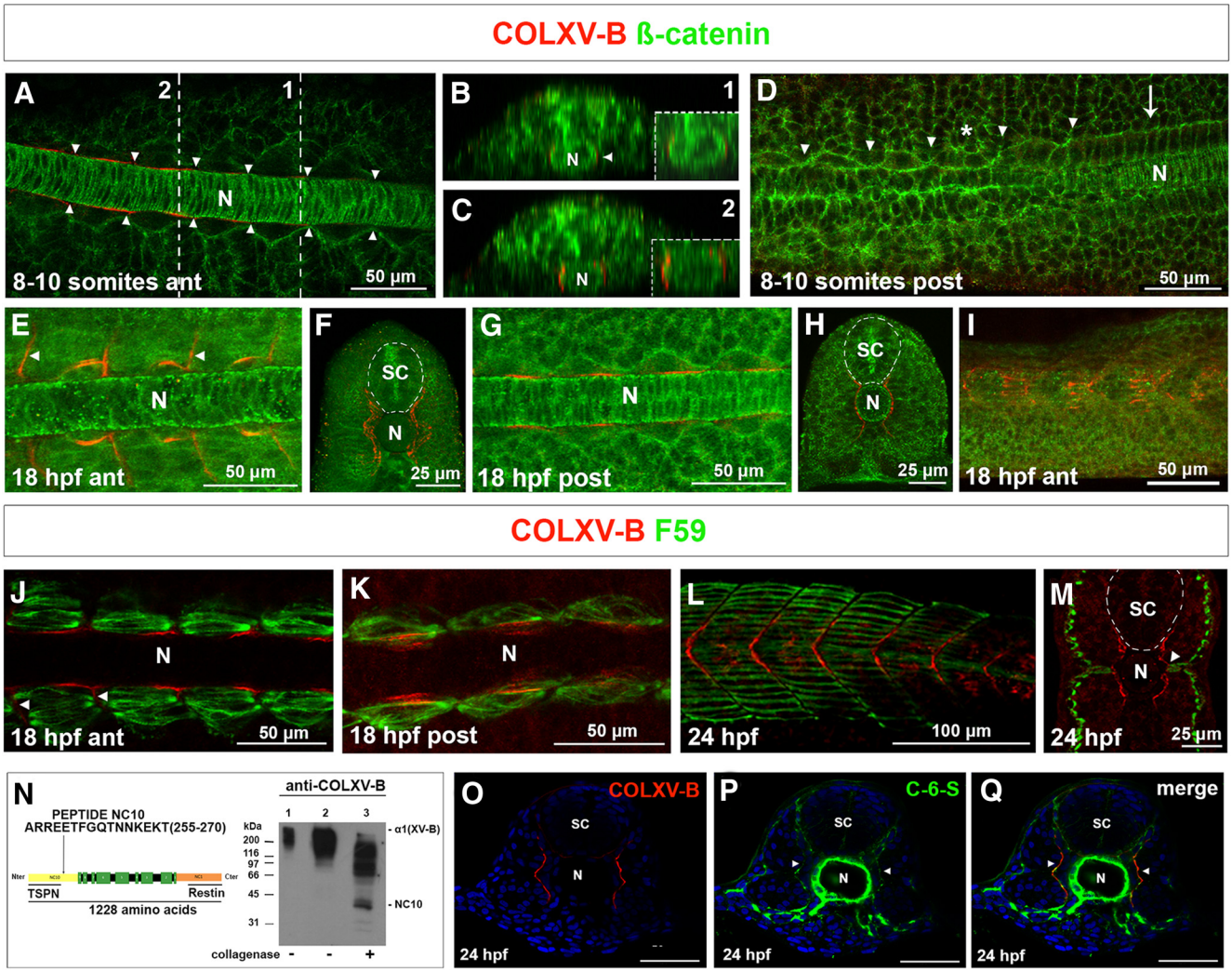

Figure 1. COLXV-B deposition during primary myogenesis. ***A–I***, Immunostaining of embryos at 8–10 somites (***A–D***) and 18 hpf (***E–I***) with COLXV-B antibodies (red) and anti-β-catenin (green). Dorsal views of anterior and posterior part of the same embryonic trunk show morphological changes of adaxial cells at 8–10 somite stage: elongated adaxial cells (***A***), cuboid adaxial cells (***D***, arrow), and interleafing stage (***D***, asterisk). ***A***, COLXV-B is deposited by elongated adaxial cells. Arrowheads indicate somite boundaries. ***B***, ***C***, Orthogonal views of areas 1 and 2 as indicated in ***A***. Dorsal views (***E***, ***G***), cross sections (***F***, ***H***), and lateral view (***I***) of anterior and posterior trunk of 18 hpf embryos. ***E***, Arrowheads indicate vertical myosepta. COLX-B is deposited in the motor path and vertical myosepta. ***J–M***, Immunostaining of embryos at 18 hpf (***J***, ***K***) and 24 hpf (***L***, ***M***) with COLXV-B antibodies (red) and F59 (green). Cross section at 24 hpf (***M***) shows the persistence of COLXV-B staining in the motor path when F59-positive slow fibers (green) have migrated to the myotome periphery. ***M***, Arrowhead indicates COLXV-B staining in contact with MPs. ***N***, Production, characterization of polyclonal antibodies against zebrafish COLXV-B. Left, Schematic representation of the domain structure of the zebrafish COLXV-B α1 chain and location of the NC10 (residues 255–270) epitope. Collagenous domains (green) are numbered from the C terminus. Black represents noncollagenous linker domains. NC10 domain contains a TSPN (thrombospondin N-terminal like domain) domain and the NC1 the restin domain. Right, Western blotting with anti-COLXV-B antibodies of conditioned HEK293 media transfected with zebrafish *col15a1b* full-length cDNA incubated with (+) or without (−) collagenase. Lane 1: no treatment; lanes 2, 3: incubated at 37°C without collagenase (lane 2) and with collagenase (lane 3). The COLXV-B α1 chain is detected as an immunoreactive band migrating >200 kDa in undigested samples incubated (lane 2) or not (lane 1) at 37°C. After collagenase digestion, the band corresponding to COLXV-B α1 chain disappears and a collagenase digestion product is observed at the expected size for NC10 domain, attesting to the specificity of the anti-COLXV-B antibodies. ***O–Q***, COLXV-B coincides with chondroitin sulfate signal in the motor path (***P***, ***Q***, arrowheads). Single confocal plane of immunofluorescence staining of 24 hpf embryo cross section with antibodies to COLXV-B (***O***, red) and C-6-S (***P***, green) and merge image (***Q***). Hoechst solution was used to reveal nuclei. SC, Spinal cord (***F***, ***H***, ***M***, dotted line); N, notochord; ant, anterior trunk; post, posterior trunk. For lateral and dorsal views, anterior is left.

purified polyclonal rabbit anti-COLXV-B antibodies (dilution 1:1000), followed by incubation with goat HRP-conjugated secondary antibodies (Bio-Rad; dilution 1:10,000), using Immun-Star WesternC (Bio-Rad) as a chemiluminescence substrate.

Collagenase digestion. Collagenase specifically digests triple helical domains while leaving intact noncollagenous domains. For the collagenase assay on culture supernatants of HEK-293 EBNA cells, 2 ml of culture supernatant was first precipitated as described above. Pellets were then resuspended in 50 μl collagenase buffer (25 mM Tris-HCl, pH 7.4, 6 mM $CaCl_2$, 0.5 M NaCl, 1 mM AEBSF). The suspension was then divided in two samples of equal volume that were incubated for 2 h at 37°C with or without 333 U/ml of collagenase (CLSPA, Worthington Biochemical). The enzyme reaction was stopped with Laemmli buffer 1× (final concentration), and heated samples were then stored at −80°C or directly loaded by SDS-PAGE for Western blot analysis, as described above.

Whole-mount immunostaining. Embryos between 13 and 72 hpf were fixed overnight at 4°C in 4% PFA in PBS and transferred to 100% methanol for storage at −20°C until use or fixed for 2 h at room temperature for immediate immunostaining. Embryos stored in methanol were progressively rehydrated in decreasing concentrations of methanol in PBT (PBS, 0.1% Tween). All embryos were then permeabilized in PBS-T (1% Triton X-100 in PBS). For 52 hpf and 72 hpf embryos, additional treatments were performed. Embryos were treated with frozen acetone (for 7 min at −20°C) and incubated with proteinase K (Roche, 12 μg/ml final concentration in PBS 1×) for 20 min. Embryos were then incubated in blocking buffer (10% sheep serum in PBS-T) and incubated with pri-

mary antibodies overnight at 4°C. After washing with PBS-T, embryos were incubated overnight at 4°C with fluorochrome-coupled secondary antibodies or α-bungarotoxin drug. Finally, after washing with PBS-T, embryos were stored at 4°C until observation.

Primary and secondary antibodies and the drug α-bungarotoxin were used at indicated dilutions in 1% sheep serum in PBS-T: rabbit polyclonal anti-COLXV-B (1:100); rabbit polyclonal anti-COLXII (1:250) (Bader et al., 2009); mouse monoclonal F59 antibody (1:10, Developmental Studies Hybridoma Bank [DSHB]); mouse monoclonal znp1 antibody (1:100, DSHB); mouse monoclonal zn8 antibody (1:400, DSHB); mouse monoclonal 4D9 antibody (1:50, DSHB); rabbit polyclonal Prox1 antibodies (1:5000, Millipore); α-bungarotoxin TRITC (10 μg/ml, Biolegend); goat anti-mouse or anti-rabbit IgG coupled to AlexaFluor-488 or AlexaFluor-546 (1:500, Invitrogen).

Immunostaining of frozen tissue sections. Embryos were fixed overnight at 4°C in 4% PFA, quickly washed with PBS, and embedded in blocks containing 1.5% agarose and 5% sucrose. Blocks were incubated overnight at 4°C in 30% sucrose in PBS, embedded in OCT freezing medium, and then snap-frozen in cold isopentane; 30 μm cryosections were cut using a Leica cryostat and stored at −80°C until use. For immunostaining, frozen sections were rehydrated for 5 min in PBS and incubated 30 min in blocking buffer (1% BSA, 3% sheep serum in PBS). Primary antibodies were then incubated for 1 h at room temperature. After quick washes in PBS, secondary antibodies or phalloidin drug were incubated for 1 h at room temperature. After a rapid wash in PBS, nuclei were stained for 5 min with 1.5 μg/ml Hoechst 33258 (Sigma). Samples were washed and mounted in 50% glycerol:PBS and stored at 4°C until imaging. Primary and secondary antibodies and phalloidin drug were used at stated dilutions in blocking buffer: mouse monoclonal anti-β-catenin antibody (1:400; Sigma); rat monoclonal anti-C-6-S antibody (1:100; Mab 473HD antibody, from Andreas Faissner, Bochum, Germany); rabbit anti-COLXV-B antibodies (1:100); goat anti-mouse or anti-rabbit IgG coupled to AlexaFluor-488 or AlexaFluor-546 (1:500; Invitrogen); goat anti-rat IgG coupled to AlexaFluor-488 (1/200; Invitrogen); and phalloidin-TRITC (1:100; Sigma).

Hh signaling forced activation. To mimic activation of the Hh pathway in the overall myotome, 50 pg of mRNA encoding the dominant negative form of PKA (dnPKA) or Sonic Hh factor (Shh) was injected at the 1-cell stage as previously described (Concordet et al., 1996; Du et al., 1997). Capped mRNA was synthesized *in vitro* using a message machine SP6 kit (Ambion) from PCS2+-dnPKA and Shh plasmids (gift from Stone Elworthy, University of Sheffield, Sheffield, United Kingdom), linearized by NotI and BamHI, respectively. Embryos derived from an incross of heterozygous *lep(ptch1)*^{tj222} and *ptch2*^{hu1602} mutants, previously shown to present an aberrant activation of Hh signaling in double homozygotes (Koudijs et al., 2008), were used.

Whole-mount RNA in situ hybridization. The following DIG-labeled probes were synthesized with Promega RNA polymerase, as previously described: *col15a1b* (Bretaud et al., 2011), *eng2a* (Ekker et al., 1992), *ptch2* (Concordet et al., 1996), and *smyhc1* (Elworthy et al., 2008). Whole-mount *in situ* hybridizations were performed as previously described (Bader et al., 2009) with the following modifications: the hybridization mix contained total RNA from Torula yeast (Sigma) purified using the phenol chloroform method; hybridization was performed at 69°C; anti-DIG-AP (Roche) antibody was diluted at 1:5000; excess of anti-DIG antibody was removed with several washes in PBT containing 2 mg/ml BSA; the staining reaction was stopped with PBT, followed by 20 min postfixation in 4% PFA; embryos were equilibrated in increasing concentrations of glycerol in PBS for observation in 75% glycerol. Transverse sections of approximately one somite thick were performed under a stereomicroscope with a razor blade at appropriate levels, depending on the experiment.

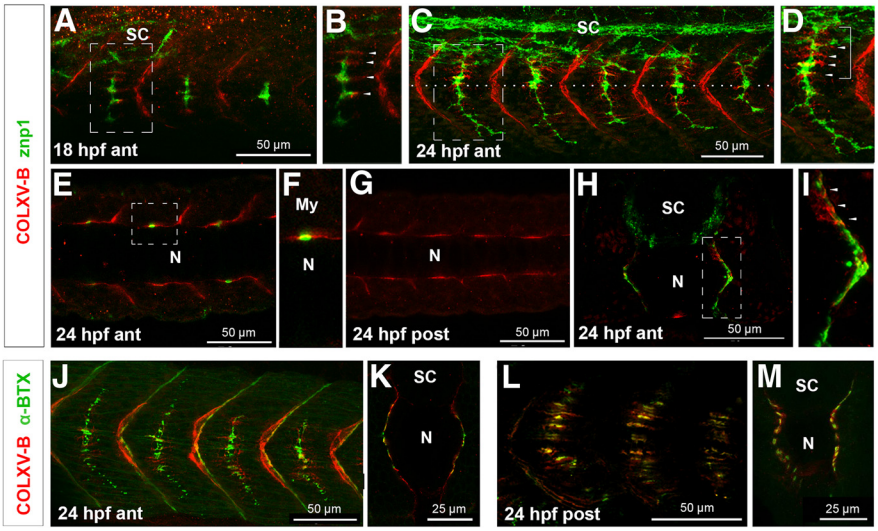

Figure 2. COLXV-B is present in the pathway of motor axons and coincides with aneural AChR clusters. Double staining of embryos at 18 hpf (***A***, ***B***) and 24 hpf (***C–M***) with anti-COLXV-B antibodies (red) and znp1 (green) to label primary motoneurons (***A–I***) or conjugated α-bungarotoxin (α-BTX, green) to stain AChR (***J–M***). ***A–D***, Lateral views of anterior mid-trunk (boxed areas in ***A***, ***C*** indicate higher magnification shown in ***B*** and ***D***, respectively). ***B***, ***D***, Arrowheads point to the ladder-type structural organization of COLXV-B staining. ***D***, Bracket represents COLXV-B signal enrichment along the common path. ***C***, Dotted line indicates the position of the horizontal myoseptum. ***E–G***, Dorsal views of anterior (***E***, ***F***) and posterior (***G***) trunk. ***F***, Higher magnification of the boxed area in ***E*** showing that COLXV-B deposit embraces CaP axon. ***H***, ***I***, Strong COLXV-B signal is observed along the common path (arrowheads) wrapping around motoneuron axon. ***H***, Cross section. ***I***, Higher magnification of boxed area in ***H***. ***J–M***, Lateral views (***J***, ***L***) and cross sections (***K***, ***M***) at the level of neural (anterior mid-trunk) and aneural clusters (posterior trunk). COLXV-B is present within the neural clusters of AChR in the anterior trunk (***J***, ***K***) and colocalizes with the aneural clusters of AChR in the posterior trunk (***L***, ***M***). N, Notochord; SC, spinal cord; My, myotome; ant, anterior mid-trunk; post, posterior trunk. For lateral and dorsal views, anterior is to the left.

Transient reporter gene expression analysis. A 2.5 kb fragment upstream of the ATG start site of the *col15a1b* gene was cloned by nested PCR from adult AB/TU gDNA. Both sets of the following primers were used: external primers, 5′-TTTTGTGGGACATTGCAGAA-3′ and 5′-ATAACCCA AGGCGAGATGTG-3′; and internal primers, 5′-GGGTCATGTAAA GCATTTG-3′ and 5′-CCTTGCTCACCATGGTGGCGAAAAAGTCAA GCATGAGATTA-3′. The last primer also contained a Kozak sequence CGCCGCCACC and a NcoI site for subcloning at the GFP level into a reporter plasmid based on the pCS2+ vector that contained the GFP and SV40-polyA sequences. The I-SceI site was also present just before insertion of the *col15a1b* promoter. The zebrafish genomic region encompassing *col15a1b* and *tgfbr1a* genes (chr2:23,834,000–24,027,000, Zv9 assembly) was searched for Gli putative binding sites using the "matrix-scan" tool from the RSAT suite (Thomas-Chollier et al., 2011) with default parameters (background model estimated from input sequences). GLI1 and GLI2 consensus binding motifs were retrieved from the TRANSFAC database (Matys et al., 2006) (matrices M01037, M01042, M01702, and M01703). The GGGTGGTC motif was found at 1726 bp upstream of the translation site. This site, present in the *col15a1b-GFP* plasmid, was mutated using site-directed mutagenesis with the QuikChangeLightning kit (Agilent Technologies), and the primers were designed according to the Agilent Technologies website: 5′-ACGTCCACAGAAGGACGAGGCGGAGGTAAGAGCC-3′ and 5′-GGCTCTTACCTCCCGCCTCGTCCTCGTGGACGT-3′. The sequence of the mutated plasmid was analyzed by GATC. Both plasmids (wt and mutated) were digested for 30 min at 37°C with I-SceI enzyme (Biolabs), and 50 pg of the digested plasmid was injected into the yolk of 1 cell-stage embryos.

Morpholino design and morpholino knockdown. The morpholino antisense strategy was performed following the recommendations of Gerety

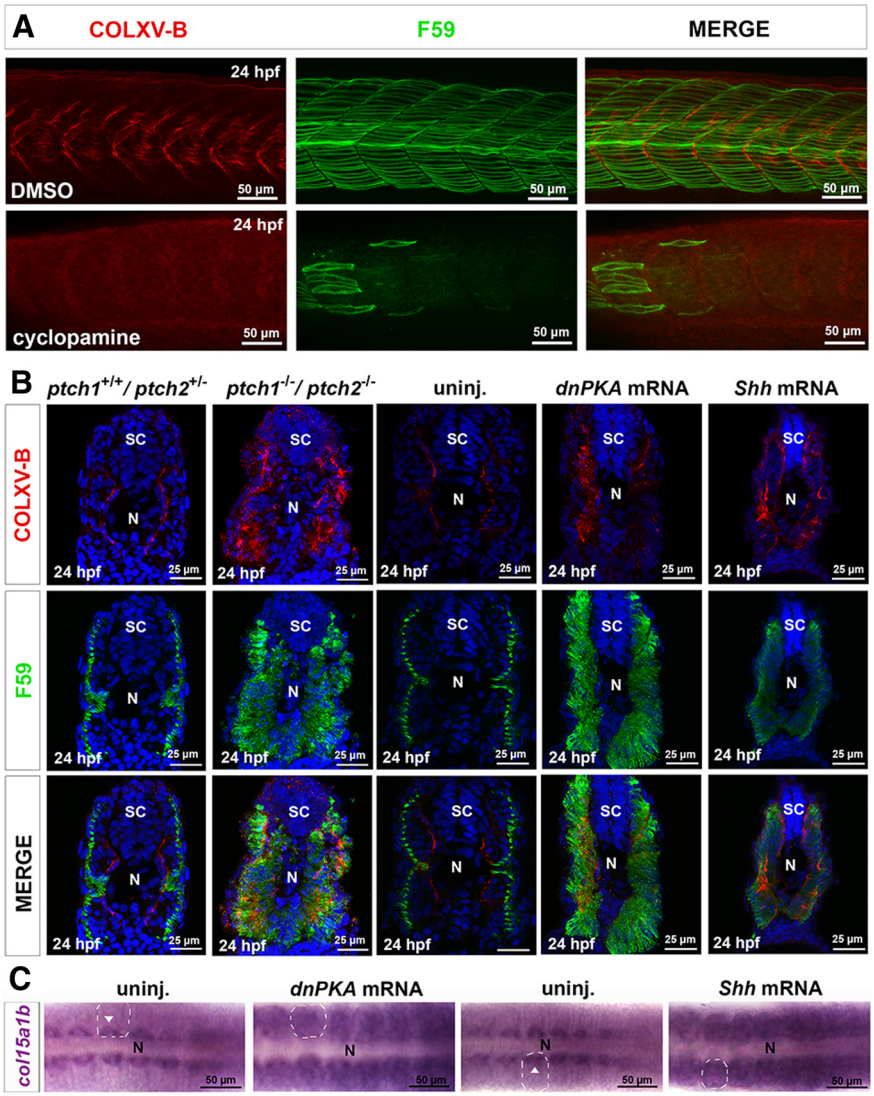

Figure 3. *col15a1b* expression in the myotome depends on Hh/Gli signaling. ***A***, Costaining with anti-COLXV-B (red) and F59 (green) of 24 hpf embryos treated with cyclopamine to inhibit HH signaling or DMSO as control. Lateral views with anterior to the left. ***B***, Costaining with anti-COLXV-B (red) and F59 (green) of 24 hpf double homozygous *ptch1* $^{-/-}$/*ptch2* $^{-/-}$ mutants and wild-type/heterozygous clutch mates *ptch1* $^{+/+}$/*ptch2* $^{+/-}$ or embryos injected with *dnPKA* or *Shh* mRNA and uninjected (uninj.) control embryos; Hoechst solution was used to reveal nuclei. Cross sections with dorsal up. ***C***, *In situ* hybridizations with *col15a1b* probe of 18 hpf dnPKA or Shh mRNA-injected embryos and uninjected (uninj.) control embryos. Dashed lines indicate the whole somite. Arrowheads indicate adaxial cells. N, Notochord; SC, spinal cord. Lateral views with anterior to the left.

and Wilkinson (2011). Morpholino antisense oligonucleotides (MOs), complementary to the translation start site of *col15a1b* mRNA (tMO15b) and to the exon 2–intron 2 boundary of *col15a1b* pre-mRNA (sMO15b), were designed and synthesized by Gene Tools (www.gene-tools.com). The 5′-3′ sequences were as follows: tMO15b AAAGTCCAAGCATG AGATTAGTGCA; sMO15b AGAGTATTCCCCTACCTTCCATGAC; 0.5 nl of each MO was injected into the vitellus of 1–2 cell stage embryos at a dose of 12.8 ng for tMO15b and 4.2 ng for sMO15b. The latter was coinjected with 1.7 ng of p53MO (Robu et al., 2007) to decrease off-target toxicity. Standard control MO (ctl-MO) provided by Gene Tools was used as a negative control in our experiments. To evaluate the efficacy of sMO15b, total RNA from 24 hpf-injected embryos ($n = 20$ embryos per condition) was isolated according to the TRIZOL method (Invitrogen). Reverse transcription was performed for 1 h at 37°C with 3 μg of RNA using oligodT, dNTP, and MMLV reverse transcriptase from Promega. PCRs were performed on 1 μl cDNA with DNA polymerase from Biolabs and the following primers (Sigma) at the annealing temperature of 60°C: 5′-TGGG TGACAACACTCTGGAA-3′ (*col15a1b*exon1 forward); and 5′-TGAAGGACACAGA-TG GTGGA-3′ (*col15a1b*exon3 reverse). PCRs were analyzed with 2.5% agarose gel electrophoresis. For sequencing, the PCR product was gel purified using the Nucleospin Extract II kit (Macherey Nagel).

Overexpression and rescue experiments. The full-length *col15a1b* was amplified from the pCS2+-*col15a1b* plasmid. NcoI and XbaI sites were added by PCR at the 5′ and 3′ ends, respectively, using the following primers: 5′-CCATGGGATTTCGCCTCCTG-3′ and 5′-C GCTCTAGACTAGTTCCTTC-3′. After digestion, the PCR product was subcloned into the *smyhc1:GFP* vector (gift from Stone Elworthy, University of Sheffield, Sheffield, United Kingdom) from which the GFP fragment was removed by NcoI-XbaI digestion. Depending on the experiment, the *smyhc1:col15a1b* plasmid was injected in 1 cell-stage embryos at 50 pg (rescue experiment) and 100 pg (overexpression) after 30 min digestion with the meganuclease Isce-I (Biolabs) to increase transgenesis efficiency (Soroldoni et al., 2009). For the rescue experiment, we used a plasmid instead of mRNA, as described previously (Takeuchi et al., 2010).

Motility assay. Responses to touch stimuli were monitored on 2 dpf embryos as described previously (Goody et al., 2012). Briefly, embryos were placed individually in a 60 mm Petri dish in the center of a 10-mm-diameter circle. Time-lapse experiments were performed with an axiozoom microscope (Zeiss). After touching embryos at the tip of the tail, the time (in milliseconds) needed to escape out of the circle was calculated. A total of 45 embryos, or 50 embryos for rescue experiment, from three independent injections were observed for each condition.

Imaging. Embryos after whole-mount *in situ* hybridization were observed and imaged using a Leica stereomicroscope MZ16 or LEICA DM/4000B light microscope equipped with a Nikon digital camera. Immunostaining was imaged with inverted confocal microscopes (Zeiss LSM 510 and LSM 780) or an SP5 spectral confocal detection microscope (Leica) available at the PLATIM facility and Institut de Génomique Fonctionnelle de Lyon (Lyon, France). Except when indicated, immunostaining images are *Z* projections of confocal *Z* stacks. Images were acquired with identical confocal settings and were equally post-treated with ImageJ software to respect differences in signal intensity.

Statistical analyses. To avoid collecting and analyzing the data in a biased fashion, blind experiments have been performed and analyzed by two independent experimenters (E.G. and S.B.). Significant effects were assessed with a two-tailed Student's test using Excel software. Data represent mean ± SEM. The Mann–Whitney test (GraphPad Prism software) was used for the quantification of fast fiber areas that showed non-normal distribution.

Results

COLXV-B is deposited early in the future axonal motor path and in vertical myosepta

Col15a1b is transiently and specifically expressed in adaxial cells (Bretaud et al., 2011). These cells, initially present next to

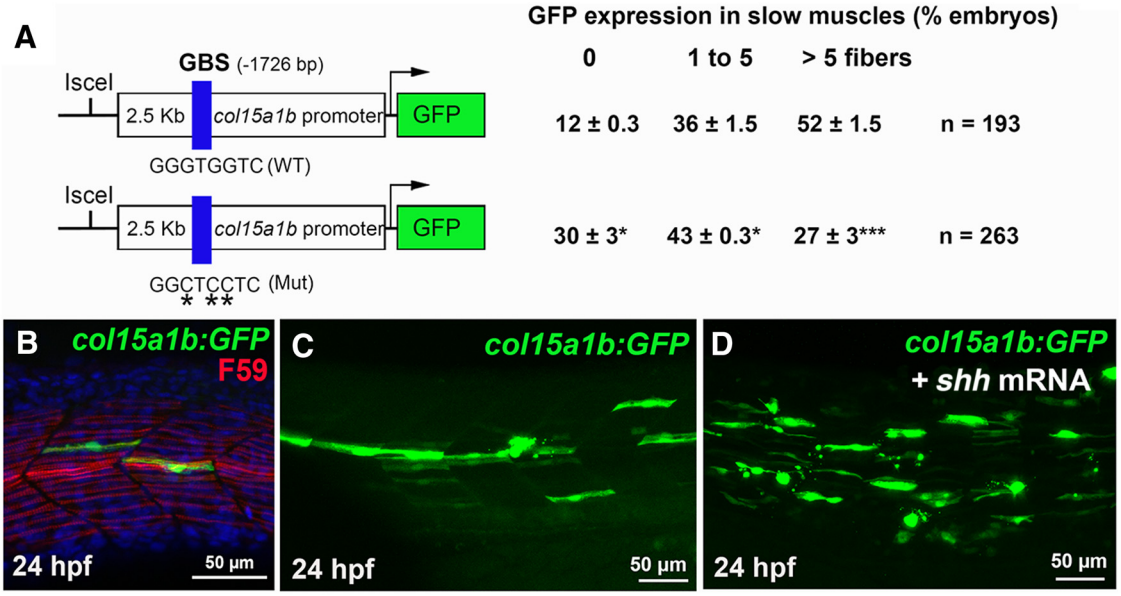

Figure 4. *Col15a1b* is expressed in slow muscle as a direct target gene of Hh signaling effectors. ***A***, Schematic representation of *col15a1b:GFP* reporter constructs driving GFP expression under the control of 2.5 kb *col15a1b* zebrafish proximal promoter encompassing the wild-type (GGGTGGTC, *col15a1b:GFP*) or mutated (GGCTCCTC; *col15a1bMut:GFP*) putative Gli binding site (GBS, blue box) at position −1726. The Icse I restriction site is indicated. GFP-transgenic embryos at 24 hpf were selected, and GFP-positive slow muscle fibers/embryo were quantified. Data are expressed as mean percentage of embryos ± SEM for three independent experiments (n = number of injected embryos). *$p < 0.05$ (Student's t test). ***$p < 0.001$ (Student's t test). ***B***, Single confocal plane at the trunk level (lateral view anterior left) of embryos injected with *col15a1b:GFP* and stained with F59 (red). Blue represents nuclei. ***C***, ***D***, GFP expression in embryos injected with *col15a1b:GFP* construct alone (***C***) or in combination with Shh mRNA to induce ectopic activation of Hedhehog signaling (***D***).

the notochord, undergo morphological changes and migrate to form a monolayer of slow superficial fibers (SSFs) on the surface of the myotome, whereas a subset of cells that do not migrate differentiates into MPs that remain in the region of the horizontal myoseptum (Daggett et al., 2007). To determine the site of collagen XV-B deposition during primary myogenesis, we raised and characterized polyclonal antibodies against COLXV-B, referred to as anti-COLXV-B; and using Western blotting, we showed that they specifically recognized the NC10 domain of the zebrafish collagen XV-B protein produced recombinantly (Fig. 1*N*). Embryos were costained with anti-COLXV-B and β-catenin to delineate cell shape (Fig. 1*A–I*) or F59 antibody to reveal slow muscle fibers (Fig. 1*J–M*). At the 8–10 somite stage, COLXV-B immunoreactivity was present rostrally just as the adaxial cells became elongated (Fig. 1*A*, *G*). COLXV-B staining delineated the outer surface of the adaxial cells on the notochord side, but only in the posterior half of the somite. Orthogonal views of two regions of the tail (marked in Fig. 1*A* as 1 and 2) showed that COLXV-B deposition started at the dorsoventral midpoint (Fig. 1*B*) where the first elongated adaxial cells localize (Nguyen-Chi et al., 2012) and further expand dorsoventrally along the notochord with somite maturation (Fig. 1*C*). COLXV-B protein was not detected in the immature somites and in presomitic mesoderm (Fig. 1*D*). When slow myoblasts initiated radial migration at 18 hpf, COLXV-B staining extended to the ventral part of the spinal cord (Fig. 1*F*). This specialized region, known as the motor path, represents the future outgrowth territory of motor axons (Bernhardt and Schachner, 2000). COLXV-B was also deposited along the vertical myosepta (Fig. 1*E*, *J*).

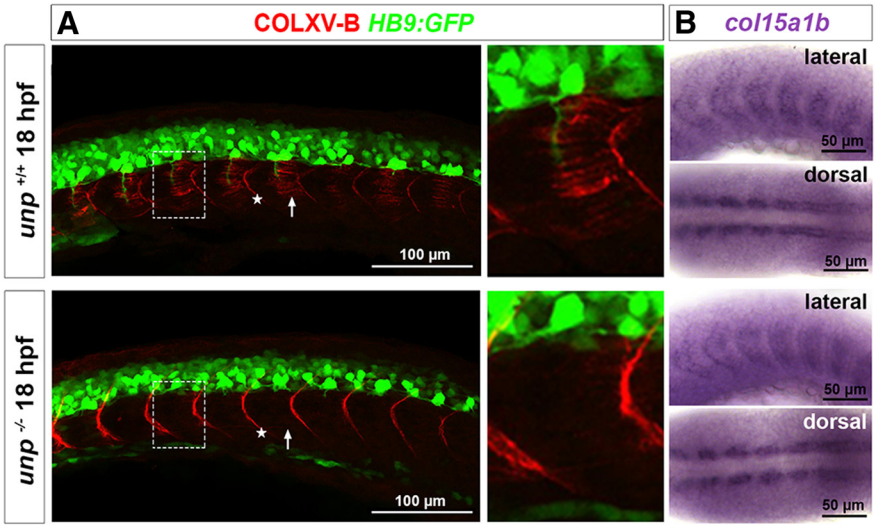

Figure 5. *unp*/MuSK signaling organizes COLXV-B deposition in the motor path. ***A***, Lateral views of 18 hpf wild-type ($unp^{+/+}$) and homozygous *unplugged* ($unp^{-/-}$) clutch mate embryos in HB9:GFP background (green) that are stained with COLXV-B antibodies (red). Arrows point to motor path. Asterisks indicate vertical myosepta. Right panels, Boxed regions at higher magnification. ***B***, *In situ* hybridizations with *col15a1b* probe of 18hpf $unp^{+/+}$ and $unp^{-/-}$ embryos. Embryos are anterior to the left.

Although *col15a1b* expression ceased at 24 hpf (Bretaud et al., 2011), we found that COLXV-B staining persisted in the motor path (Fig. 1*L*, *M*) and in the central part of the vertical myosepta (Fig. 1*L*) and that MPs remained in close contact with COLXV-B on the notochord side (Fig. 1*M*). In the motor path, COLXV-B was strikingly present at regular intervals in a ladder-like structure (Fig. 1*I*, *L*). CSPGs are components of the motor path (Bernhardt and Schachner, 2000). Coimmunostaining of 24 hpf

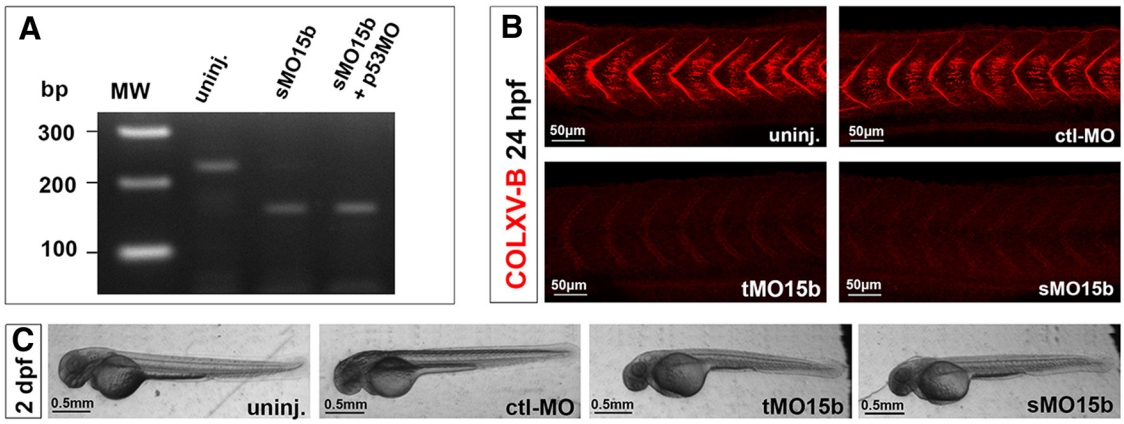

Figure 6. *col15a1b* morpholino-knockdown efficiency. ***A***, Analysis of *col15a1b* transcripts by RT-PCR in 24 hpf uninjected and injected embryos with splice-blocking morpholino (sMO15b) alone or in combination with p53MO. The shift in size of the PCR product corresponds to exon 2 skipping (as verified by sequencing). ***B***, COLXV-B staining of 24 hpf uninjected embryos (uninj.) and embryos injected with standard morpholino (ctl-MO), morpholino targeted to the ATG site (tMO15b), or to exon 2 splicing (sMO15b). No COLXV-B immunoreactivity is observed in MO15b-injected embryos. Pictures are acquired with identical confocal settings and are equally post-treated with ImageJ to respect differences in signal intensity. ***C***, Bright-field images of 2 dpf uninjected embryos (uninj.) or embryos injected with standard morpholino (ctl-MO), morpholino targeted to the ATG site (tMO15b), or splice-blocking morpholino (sMO15b) in combination with p53MO (sMO15b) showing no morphological defects or developmental delay. Lateral views with anterior to the left.

embryos with anti-COLXV-B (Fig. 1*O*) and anti-chondroitin-6-sulfate chains (473HD) (Fig. 1*P*) confirmed that COLXV-B formed part of the ECM present along the motor path (Fig. 1*Q*). We conclude that COLXV-B deposition correlates with adaxial cell elongation and that this ECM protein is deposited along the motor path before adaxial cell migration and persists in this region thereafter.

COLXV-B paves the way for CaP axons and concentrates at aneural clusters

The presence of COLXV-B along the CaP axon trajectory was confirmed by znp1 staining (Fig. 2*A*–*I*). When CaP axons had nearly reached the ventral edge of the myotome at 24 hpf, COLXV-B was highly enriched along the common path and at the choice point (Fig. 2*C*,*D*). COLXV-B lined the myotomal side of the CaP axon and was deposited in the axon trajectory before the arrival of CaP axons (Fig. 2*E*,*G*). Thus, COLXV-B is clearly part of the physical matrix path in which growing CaP axons navigate (and with which they interact) in their way to the myotome since their exit from spinal cord. Interestingly, COLXV-B staining seems to coincide with the axon varicosities where axons make synaptic contacts (Fig. 1*B*,*D*). We thus used α-bungarotoxin as an aneural and neural acetylcholine receptor (AChR) cluster marker to confirm the localization of COLXV-B at the nascent neuromuscular junction (Fig. 2*J*–*M*). COLXV-B decorated the region where neural clusters had formed and was particularly enriched at the choice point where large AChR clusters were observed (Fig. 2*J*,*K*). In the most caudal somites, COLXV-B staining coincided with aneural AChR clusters (Fig. 2*L*,*M*). We conclude that deposition of COLXV-B marks out the position of aneural clusters and persists in this region at the time of neural cluster formation.

Expression and extracellular deposition of *col15a1b*/COLXV-B in the motor path depend on a two-step mechanism involving Hh/Gli and MuSK signaling

We next wanted to determine the molecular signal that controlled *col15a1b* expression in adaxial cells. In zebrafish, specification of the different muscle cell types is mainly controlled by Hh factors. Cyclopamine treatment resulted in a complete loss of *col15a1b* expression (Bretaud et al., 2011) and protein staining (Fig. 3*A*), suggesting that Hh signaling regulates *col15a1b* expression. Double homozygous *ptch1/ptch2* mutants showed an aberrant activation of Hh signaling that resulted in conversion of the entire myotome into slow muscle cells (Koudijs et al., 2008). We thus analyzed COLXV-B localization in *ptch1/ptch2* mutants. As expected, intense COLXV-B staining was observed throughout the whole myotome in the $ptch1^{-/-}/ptch2^{-/-}$ mutants ($n = 6$), whereas wild-type/heterozygous clutch mates displayed normal COLXV-B staining ($n = 36$) (Fig. 3*B*). We confirmed this result at both the transcriptional (Fig. 3*C*) and protein levels by injecting mRNA encoding dnPKA or Shh (Fig. 3*B*). We conclude that *col15a1b* participates in the slow muscle genetic program that is activated in adaxial cells in response to Hh signaling.

We next investigated whether *col15a1b* is a direct target gene of Hh/Gli signaling. Bioinformatic analysis of the genomic region (UCSC genome browser, Zv9 assembly), upstream of the *col15a1b* translation start site, identified a putative Gli binding site (GBS) GGGTGGTC at position −1726 pb. We generated a reporter construct (*col15a1b:GFP*) with *GFP* under the control of the 2.5 kb proximal region of the *col15a1b* promoter and a GBS-disrupted mutant of *col15a1b:GFP* (*col15a1bMut:GFP*) (Fig. 4*A*). Injection of *col15a1b:GFP* into one-cell embryos resulted in a strong GFP expression restricted to F59-positive slow muscle fibers at 24 hpf (Fig. 4*B*). Coinjection with *Shh* mRNA showed a substantial expansion of the GFP expression domain in the myotome compared with embryos injected with *col15a1b:GFP* alone (Fig. 4*C*,*D*). The proximal 2.5 kb region of the *col15a1b* promoter was thus sufficient to drive *col15a1b* expression in slow muscle fibers upon Shh signaling. To further investigate the functionality of the putative GBS sequence, embryos were injected with the mutated construct. Injected embryos displayed significantly less GFP-positive slow muscle fibers at 24 hpf than when injected with the wild-type construct (quantification in Fig. 4*A*). Together, these data demonstrate that *col15a1b* is a transcriptional target of Hh/Gli signaling in slow muscle fibers.

Unplugged/MuSK signaling has been shown to mediate growth cone guidance by organizing deposition of ECM components (tenascin-C and CSPG) in the motor path (Zhang et al., 2004; Schweitzer et al., 2005). We thus reasoned that *unplugged*/MuSK signaling might be responsible for COLXV-B deposition and organization in this region. To test this hypothesis, we im-

munostained COLXV-B in 18 hpf embryos derived from incrossed *unp* heterozygotes in an HB9:GFP background to visualize motoneurons. We observed that COLXV-B immunoreactivity was completely absent from the motor path in *unp* homozygous embryos ($n = 15$), but present in vertical myosepta, with an even stronger staining intensity than in control embryos ($n = 40$; Fig. 5*A*). In contrast, expression of *col15a1b* in $unp^{-/-}$ embryos was unchanged compared with $unp^{-/+}$ and wild-type clutch mates (Fig. 5*B*). We conclude that *unplugged*/MuSK signaling acts specifically on COLXV-B deposition and organization in the motor path without affecting *col15a1b* expression and protein deposition in the vertical myosepta. Together, these data show that *col15a1b* expression and subsequent protein deposition in the motor path depend on two independent but successive signaling pathways, Hh/Gli and MuSK.

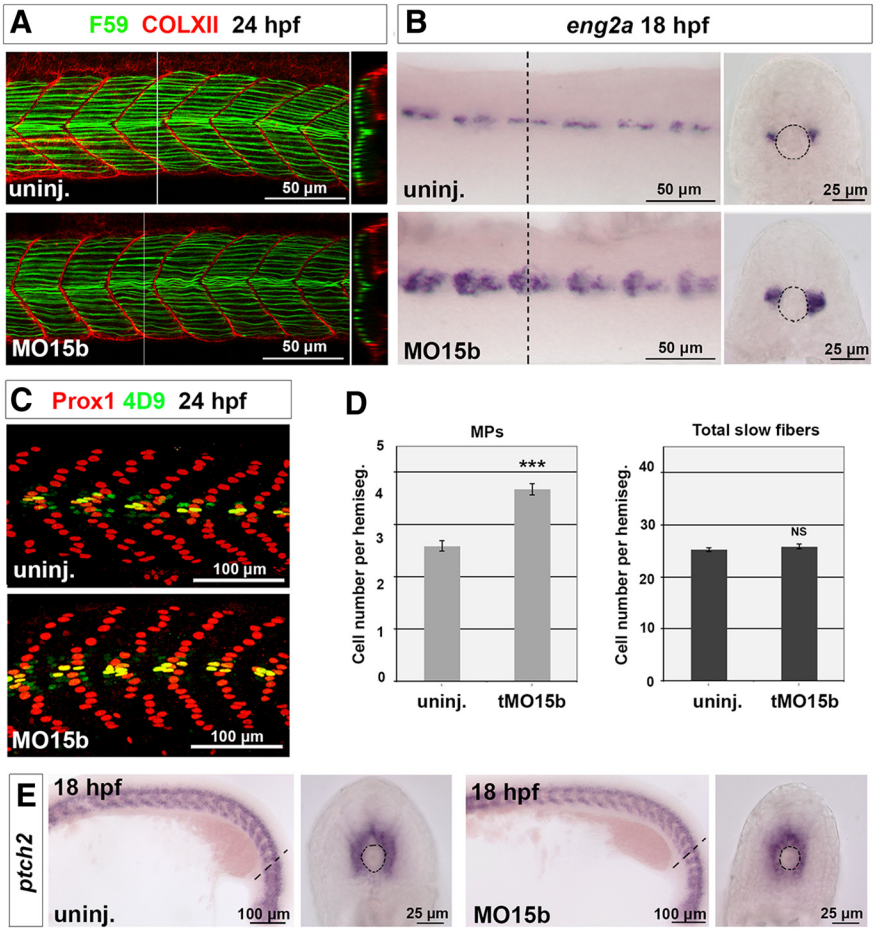

Figure 7. COLXV-B influences MP fate. ***A***, Immunofluorescence of 24 hpf uninjected (uninj.) and MO15b-injected (MO15b) embryos with F59 (green) and collagen XII antibodies that stain vertical myosepta (COLXII, red). Orthogonal views at the level of the white line in ***A***, ***B*** (right panels) show positions of migrated SSFs that were not affected in morphants (green). ***B***, *In situ* hybridization of 18 hpf uninjected and MO15b-injected embryos with the MP marker *engrailed2a* (*eng2a*) probe. ***C***, Immunostaining of 24 hpf uninjected and MO15b-injected embryos with the slow muscle marker Prox1 (red) and 4D9 (engrailed, green) antibodies that mark SSFs (red), MPs (yellow), and medial fast fibers (green) nuclei. ***D***, Quantification of MP number (left) and total number of slow muscle cells (right, MPs + SSFs) per somite hemisegment of 24 hpf tMO15b-injected (n hemisegments = 56) and uninjected embryos (n hemisegments = 59) confirms an increase in the number of MPs in morphants. Data are mean ± SEM. NS, Nonsignificant. ***$p < 0.001$ (Student's t test). ***E***, *In situ* hybridization of 18 hpf uninjected and MO15b-injected embryos with the *patch2* receptor (*ptch2*) probe, a direct target of Hh signaling. Lateral views with anterior to the left. Cross sections were prepared at the position indicated by the dashed line in the corresponding lateral view.

COLXV-B contributes to the regulation of MP cell fate

To further investigate the role of *col15a1b* in developing zebrafish, we designed two distinct morpholinos, tMO15b and sMO15b, targeting, respectively, the ATG start site and the exon 2–intron 2 boundary site, and assessed their efficiency and specificity (Fig. 6). The efficacy of sMO15b was assessed by RT-PCR on RNA extracts of 24 hpf injected and uninjected embryos. PCR product analysis and sequencing confirmed correct splicing of exon 2 (Fig. 6*A*). Moreover, injection of sMO15b or tMO15b resulted in complete absence of COLXV-B immunoreactivity in 24 hpf embryos (Fig. 6*B*). Embryos injected with sMO15b or tMO15b did not provoke gross morphological defects or developmental delays (Fig. 6*C*). All experiments were performed with tMO15b- and sMO15b-injected embryos and will be thus referred to as the MO15b condition, except for statistical analyses and when indicated.

As *col15a1b* was specifically expressed by differentiating adaxial cells, we reasoned that a lack of COLXV-B might perturb their differentiation into slow muscle fibers. However, no overt differences in slow muscle fiber differentiation and localization were observed between MO15b-injected embryos and controls (Fig. 7*A*). We next wondered whether *col15a1b* knockdown could affect MP formation because COLXV-B was localized in the MP region. We found that MO15b-injected embryos showed a broader expression of the MP marker *engrailed2a* (*eng2a*) compared with controls (Fig. 7*B*). Consistent with this observation, a significant increase in the number of Prox1/4D9-positive MP cells, but not in the total number of slow fiber Prox1-positive cells, was found in *col15a1b*-morphants compared with controls, suggesting that the increase in MPs occurs at the expense of the SSFs (Fig. 7*C*,*D*). Adaxial cells that received high levels of Hh signaling differentiated into MPs. Hh receptor *ptch2* reflects Hh signaling activation in cells. No change in the *ptch2* expression domain was observed between morphants and controls (Fig. 7*E*). We conclude that COLXV-B is not required for the differentiation of adaxial cells into slow muscle fibers but does contribute to the MP-SSF balance, most likely through an Hh-independent mechanism.

COLXV-B contributes to primary and secondary motoneuron axonal pathfinding

The presence of COLXV-B in the motor path at the time of axon growth suggested a role for COLXV-B in axonal pathfinding. We thus stained 27 hpf MO15b-injected embryos with znp1 to label CaP axon stereotyped trajectories (Fig. 8A). *Col15a1b* knockdown provoked CaP axon truncation, which generally stalled at the choice point (Fig. 8*A*, quantification in Fig. 8*B*). More occasionally, CaP axons failed to exit from the spinal cord (Fig. 8*A*). To confirm our results, we used the *col15a1b* mutant strain ($col15a1b^{sa12573}$ allele) available through the European Zebrafish Resource Center (Eggenstein-Leopoldshafen, Germany) that

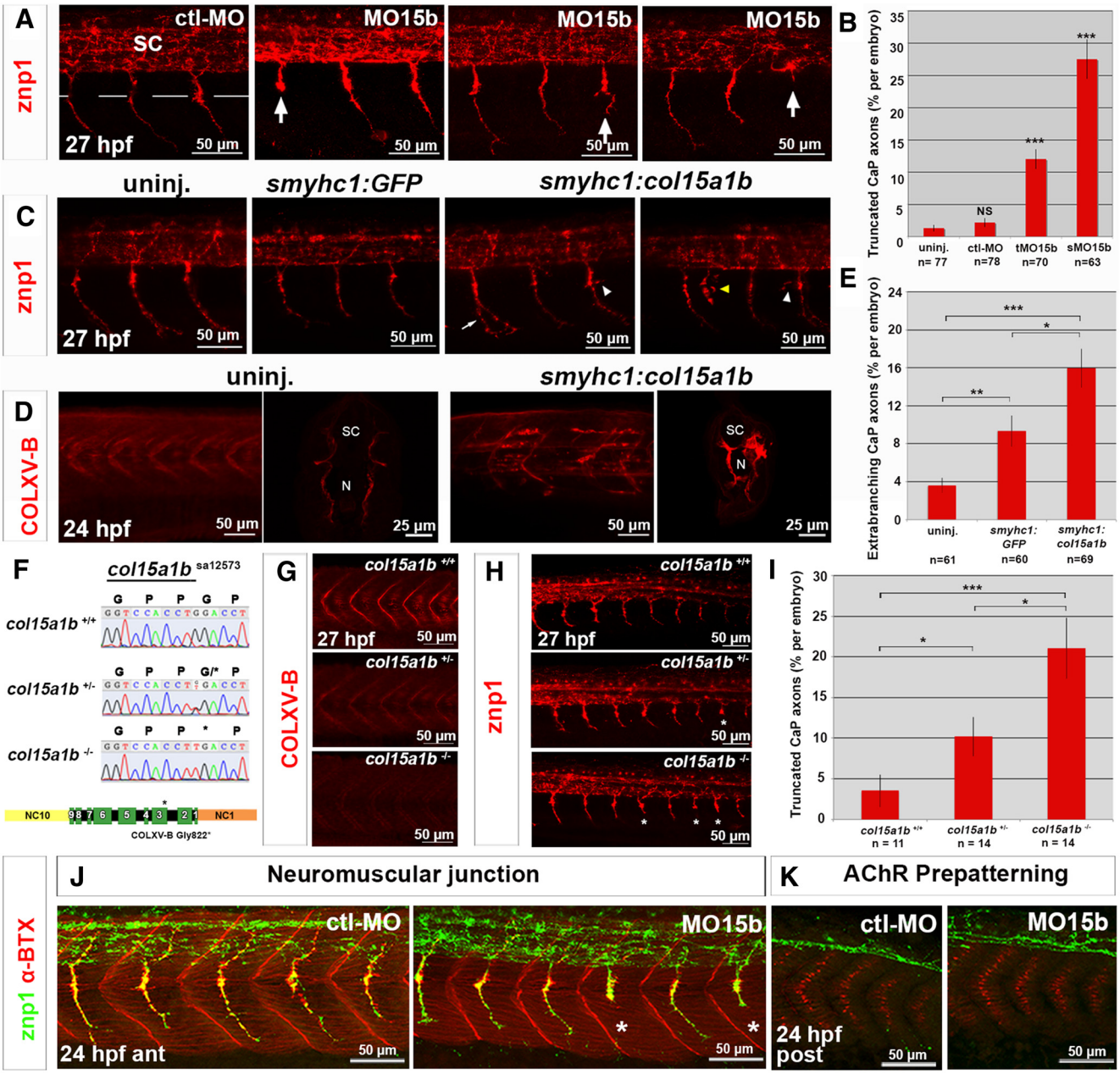

Figure 8. Loss and gain of *col15a1b* expression provokes pathfinding errors in primary motor axons. ***A***, ***B***, *col15a1b* knockdown. ***A***, Immunofluorescence of 27 hpf embryos injected with ctl-MO or MO15b with znp1 antibody to reveal primary motoneuron axons. Arrows point to axon navigation defects in MO15b-injected embryos. CaP axons stall at choice point, branch at this level, or do not exit from spinal cord. Dashed line in embryo injected with ctl-MO indicates the level of horizontal myoseptum. All embryos are lateral views. ***B***, Quantification. ***C–E***, *col15a1b* overexpression. ***C***, Embryos injected with *smyhc1:col15a1b* construct, with *smyhc1:GFP* construct, or uninjected as controls stained at 27 hpf with znp1 antibody. znp1-positive CaP axons of transgenic embryos show aberrant branches at the choice point (white arrowheads), early branching (arrow), and presence of an additional axon (yellow arrowhead). ***D***, Lateral views and cross sections of 24 hpf uninjected embryos or injected with *smyhc1:col15a1b* stained with anti-COLXV-B. ***E***, Quantification. ***B***, ***E***, For quantification, 10 hemisegments were analyzed in each embryo. ***F–I***, *col15a1b* mutants. DNA sequencing chromatograms (***F***) and immunofluorescence with COLXV-B antibodies (***G***, single confocal planes are shown) or znp1 (***H***) of 27 hpf wild-type (*col15a1b*$^{+/+}$), heterozygote (*col15a1b*$^{+/-}$), and homozygote (*col15a1b*$^{-/-}$) fish derived from incross of *col15a1b*^{sa12573} heterozygotes. A single base change (G/T) results in the introduction of a premature stop codon in the *col15a1b* ORF that is predicted to lead to truncation of COLXV-B at position 822 (***F***, asterisk). ***I***, Quantification. Eighteen hemisegments were analyzed in each embryo. For all quantification, error bars are the SEM. ***J***, ***K***, Double staining of 24 hpf ctl-MO and MO15b-injected embryos with α-bungarotoxin (red) and znp1 (green) imaged at the anterior (***J***; ant) and posterior (***K***; post) trunk levels showing that lack of COLXV-B does not affect AChR prepatterning and neuromuscular junction formation. Asterisks indicate absence of AChR clusters at the level of truncated CaP axons. Lateral views with anterior to the left. *$p < 0.05$, **$p < 0.01$, ***$p < 0.001$ (Student's *t* test). NS, Nonsignificant.

carries a nonsense point mutation (G/T). This mutation results in a premature stop in the exon 30 *of col15a1b* and predicting truncation of the protein at position 822 (Fig. 8*F*). Embryos derived from an incross of heterozygote *col15a1b*^{sa12573} fish were examined with regard to COLXV-B immunoreactivity at 27 hpf (Fig. 8*G*), and each embryo was then processed for genotyping (Fig. 8*F*). A total absence of COLXV-B staining was observed in homozygous embryos (*col15a1b*$^{-/-}$), whereas heterozygous embryos showed intermediate level of COLXV-B immunoreactivity (*col15a1b*$^{+/-}$) compared with wild-type (Fig. 8*G*). Because the COLXV-B antibodies recognized the N-terminal end of the protein, our data demonstrate that the mutation results in a com-

plete disruption of protein production. Immunostaining of 27 hpf *col15a1b*^{sa12573} embryos with znp1 confirmed that loss of function of *col15a1b* results in the significant appearance of truncated CaP axons (Fig. 8*H*, and quantification in Fig. 8*I*) similar to those observed in *col15a1b*-morphants (Fig. 8*A*). Intermediate phenotype was observed in *col15a1b*^{sa12573} heterozygote embryos (Fig. 8*H*), indicative of a dose-effect of COLXV-B. We next performed a gain of expression by injecting in one-cell embryos the *smyhc1:col15a1b* construct designed to express *col15a1b* under the control of the slow muscle specific promoter *smyhc1* (Fig. 8*C*). Injection of *smyhc1:col15a1b* resulted in a specific accumulation of COLXV-B in the motor path (Fig. 8*D*) and led to aberrant branching of CaP axons at the choice point (lateral extra-branches or division in two branches) in 15.9% of the hemisegments analyzed (Fig. 8*C*, quantification in Fig. 8*E*). Additional CaP axon exits from the spinal cord have been observed but very rarely (2 of 69 embryos examined) (Fig. 8*C*). Thus, both loss and gain of *col15a1b* expression provide evidence that COLXV-B contributes to CaP axon pathfinding at the choice point. In contrast, despite COLXV-B immunoreactivity in the environment of aneural AChR clusters and nascent neuromuscular junction (Fig. 2), COLXV-B was found dispensable for neuromuscular junction formation (Fig. 8*J*) and AChR prepatterning (Fig. 8*K*).

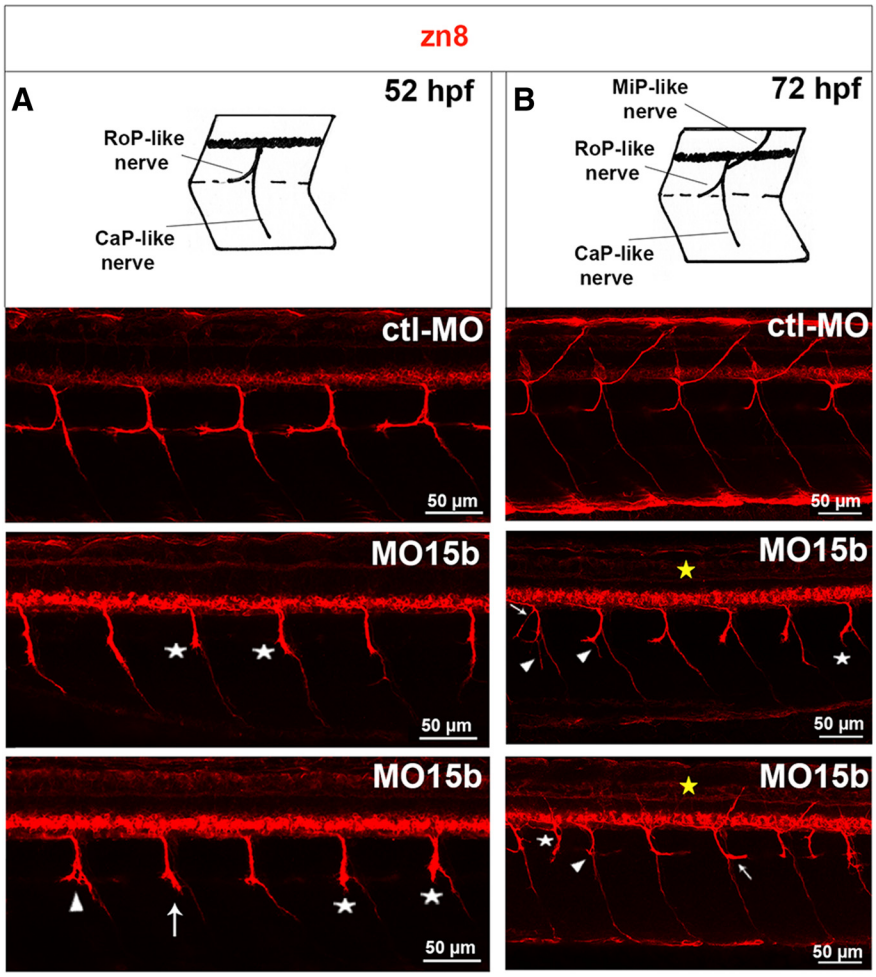

Figure 9. Lack of COLXV-B compromises secondary motor axon navigation. Immunostaining with zn8 antibody of 52 hpf (***A***) and 72 hpf (***B***) embryos injected with ctl-MO or MO15b. Diagrams depicting regular trajectories of RoP-, MiP-, and CaP-like nerves at 52 and 72 hpf. ***A***, *Abnormal extension of RoP-like nerves. Arrowheads indicate axon failure to separate properly at the choice point; arrow points to absence of CaP-like nerves. ***B***, MO15b, Top, Asterisk and arrowheads indicate respective abnormal ventral projection or additional ventral branching of RoP-like nerves; arrow indicates branching of common nerves. MO15b, Bottom, *Ectopic nerve exit from the spinal cord. Arrow and arrowhead indicate caudal projections and absence of RoP-like nerves, respectively. Yellow asterisks indicate absence of MiP-like nerves. All lateral views, anterior to the left.

The development of secondary motoneurons recapitulates the development of the pMN (Beattie, 2000). At 52 hpf, the CaP-like and RoP-like nerves had already extended toward their respective innervation territories (Fig. 9*A*). Knockdown of *col15a1b* severely affected RoP-like navigation at and past the choice point, as >65% of *col15a1b* morphant hemisegments lacked zn8-positive RoP-like nerves. More rarely, CaP-like nerves failed to project ventrally (Fig. 9*A*; Table 1). At 72 hpf, in the absence of COLXV-B, MiP-like nerves failed to project dorsally and RoP-like nerves showed significant pathfinding errors at the choice point, such as abnormal ventral axon projection and branching (Fig. 9*B*; Table 1). Occasional multiple nerve exits were observed, although not significant after quantification (Fig. 9*B*). We conclude that COLXV-B is deposited in the common motor path to influence primary and secondary axon pathfinding at the choice point.

Col15a1b knockdown causes muscle atrophy and impaired swimming performance of embryos

As muscle homeostasis depends on proper innervation, we reasoned that the defects observed in axon pathfinding could result in defective muscle stimulation and eventually muscle atrophy. Cross sections of 72 hpf larvae were thus stained with rhodamine-phalloidin to reveal the myofibril content and antibodies to β-catenin to delineate the sarcolemma (Fig. 10*A*). A significant reduction in fast fiber size was associated with a visible reduction in the myofibril content of MO15b-injected embryos, compared with controls (Fig. 10*C*). In addition, *smyhc1*-positive SSFs of *col15a1b* morphants displayed an abnormally broad shape (Fig. 10*B*). It is possible that the overall reduction in fast fiber size and myofibril content results in a decreased physical constraint at the periphery of the myotome.

These observations prompted us to examine whether innervation defects alter embryonic motility, using a specific touch-evoked assay (Goody et al., 2012). After stimulation of the tail tip, control embryos moved away immediately from the stimulus source and rapidly out of the circle (Fig. 11*A*). In contrast, repeat stimulations were often necessary to induce a swimming movement long enough for MO15b-injected embryos to be able to move out of the circle (Fig. 11*A*). In addition, their trajectory was erratic and intermittent compared with controls. As such, they moved significantly slower than control embryos (quantification in Fig. 11*B*). Importantly, the swimming phenotype was partially rescued by coinjecting tMO15b and *smyhc1:col15a1b* into one-cell embryos (Fig. 11*A*, bottom row, quantification in Fig. 11*C*). One possible scenario could be that a COLXV-B deficit results in

Table 1. Secondary motoneuron defects in *col15a1b* morphants[a]

	52 hpf		72 hpf						
	Total	RoP-like nerve	Total	RoP-like nerve			MiP-like nerve	CaP-like nerve	Common nerve
	embryos	Absence	embryos	Absence	Ventral projection	Branching	Absence	Absence	Branching
Uninjected	49	19.59 ± 4.04	44	15.45 ± 2.92	0.45 ± 0.32	0.23 ± 0.23	0.68 ± 0.38	0	0.23 ± 0.23
Ctl-MO	50	12.85 ± 2.31 (NS)	47	6.80 ± 1.58 (NS)	0.43 ± 0.29 (NS)	0.43 ± 0.30 (NS)	1.48 ± 0.6 (NS)	0.21 ± 0.21 (NS)	3.40 ± 1.15**
tMO15b	51	85.88 ± 3.79***	52	27.5 ± 3.73*	9.03 ± 2.0***	11.35 ± 2.18***	59.04 ± 6.08***	5.19 ± 2.10*	6.35 ± 1.40***
sMO15b	47	68.94 ± 5.07***	44	29.32 ± 4.12**	2.05 ± 0.62*	2.95 ± 0.90***	39.09 ± 5.90***	3.18 ± 1.48*	5.23 ± 1.36***

[a]Quantitative analysis of secondary motor axon/nerve defects per embryo under the different conditions. Results are expressed as mean frequencies of affected hemisegments per embryo ± SEM; 10 hemisegments per embryo were examined. NS, Nonsignificant.

*$p < 0.05$; **$p < 0.01$; ***$p < 0.001$; Student's *t* test.

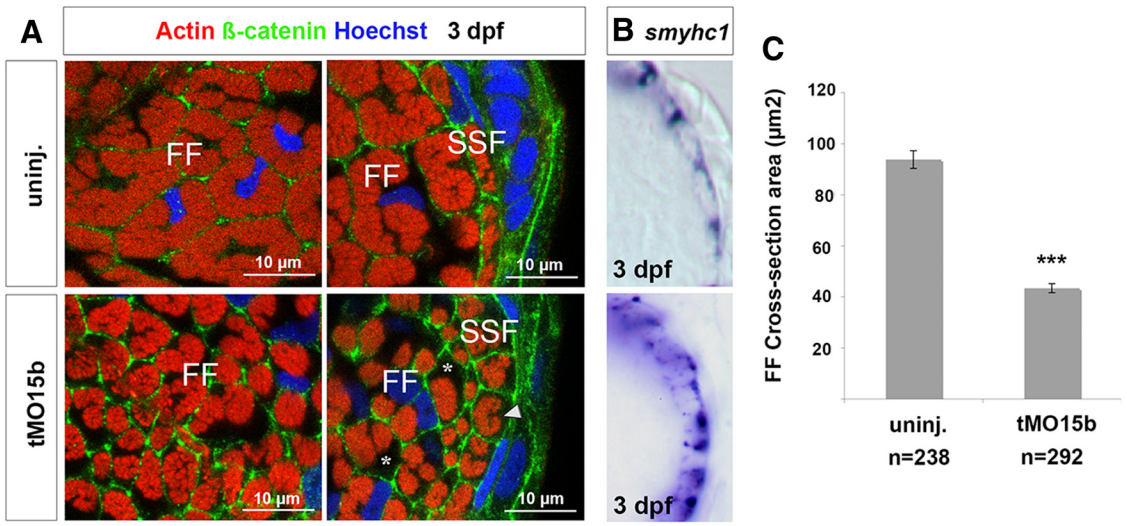

Figure 10. Knockdown of *col15a1b* results in skeletal muscle atrophy. ***A***, Triple fluorescence staining with conjugated phalloidin to visualize actin (red), β-catenin antibody to label cell membrane (green), and Hoechst solution to stain nuclei (blue) of 3 dpf uninjected (uninj.) and tMO15b-injected embryos (tMO15b). Trunk cross sections represent the center (left) and the periphery (right) of the myotome. tMO15b-injected embryos show drastic reduction of myofibril content (asterisks compared with control), a significant decrease in fast fiber (FF) size, and an abnormal shape of SSFs. ***B***, Cross sections of whole-mount *in situ* hybridization of 3 dpf uninjected and tMO15b-injected embryo probed with the slow fiber marker *smyhc1* confirming the broader shape of slow fibers in morphants. ***C***, Quantification of cross-sectional areas of individual fast fibers from 1/4 of the total myotome surface in uninjected and tMO15b-injected embryos (n = number of cells from 5 separate embryos). ***$p < 0.001$ (Mann–Whitney's test). Cross sections at the level of the yolk extension; dorsal to the top.

defective motoneuron axon pathfinding, making it impossible for axons to reach their appropriate muscle targets. The ensuing reduction in muscle excitation could then lead to muscle atrophy and eventually impair swimming performance.

Discussion

The regulatory mechanisms involved in the biosynthesis of nonfibrillar collagens are poorly documented. Hh signaling is required for muscle precursors to commit to the slow muscle fate in zebrafish (Jackson and Ingham, 2013). By compromising Hh signaling with cyclopamine, we identified a possible positive role for Hh signaling in *col15a1b* expression in adaxial cells (Bretaud et al., 2011). By modulating different Hh signaling pathway components (ligand, receptors, and intracellular effectors), we demonstrate that *col15a1b* participates in the slow muscle genetic program induced by Hh signaling. Gli transcription factors are mediators of Hh signaling that bind with high affinity to consensus sequences (Milla et al., 2012). We show that the GBS sequence GGGTGGTC located in the proximal region of the *col15a1b* promoter is responsible for *in vivo col15a1b* expression in adaxial cells. *Col15a1b* is thus a direct transcriptional target of Hh/Gli signaling. Other transcriptional factor binding sites (sp1, pea3) have been identified in the promoters of human and mouse COLXV genes (Eklund et al., 2000). The Gli-dependent expression of *col15a1b* could be a specific adaptation to the zebrafish system, in which slow *versus* fast muscle specification is orchestrated by Hh in contrast to amniotes (Jackson and Ingham, 2013).

Abnormal ECM organization was observed in the motor path of the zebrafish *unp/MuSK* mutant (Zhang et al., 2004). Immunoreactivity of the glycoprotein tenascin-C (Schweitzer et al., 2005) and chondroitin sulfate, but not laminin and heparan sulfate (Zhang et al., 2004), was markedly reduced in *unp/MuSK* mutants. We show here that MuSK signaling is additionally responsible for the deposition of a yet unreported class of ECM components in the motor path: collagen. In addition, we underscored the essential role for MuSK signaling in the organization of ECM in the motor path by showing that in *unp* mutants: (1) expression of the *col15a1b* transcript is unchanged; and (2) COLXV-B deposition by adaxial cells at the vertical myosepta is independent of the MuSK signal. Together, we have identified a novel two-step mechanism of collagen biosynthesis (Fig. 12) and highlighted the importance of this mechanism for axogenesis *in vivo*. Fundamentally, our data emphasize the critical role of adaxial cells in the control of motor axon growth, by leaving behind a matrix fingerprint that is later important for axons to navigate toward their target. The *unplugged*/MuSK signaling could be responsible for the organization of a limited set of ECM components that are probably interacting partners of the same matrix

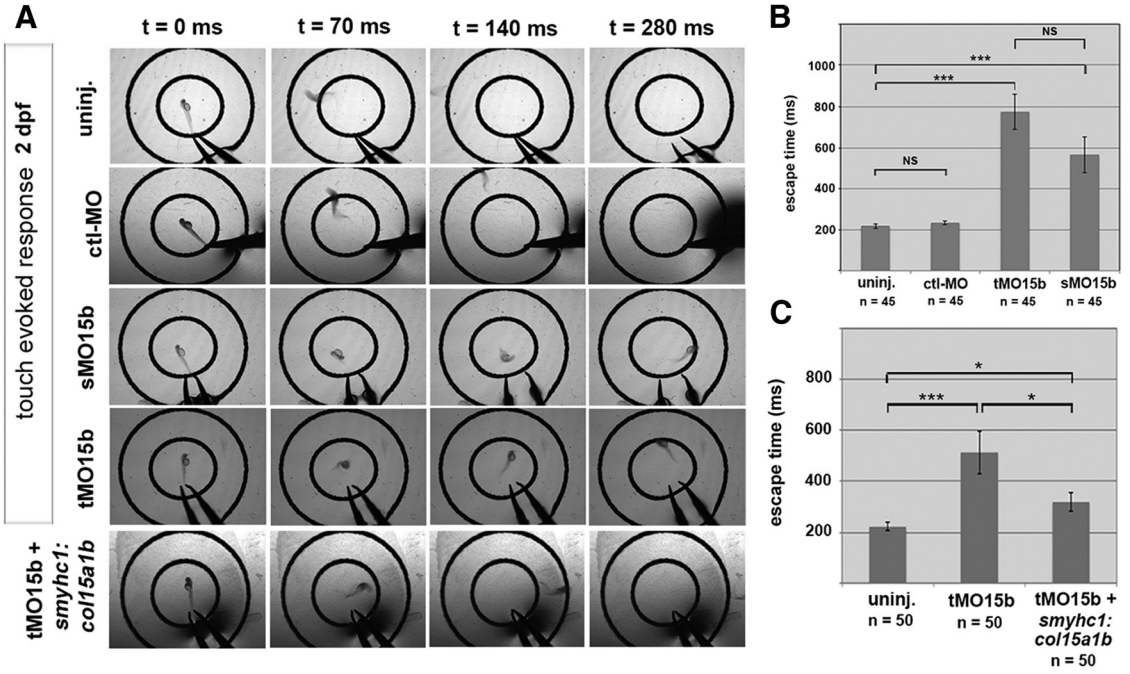

Figure 11. *Col15a1b* knockdown impairs embryo motility. ***A***, Single frame from videos showing escape response upon tactile stimulus of 2 dpf controls (uninjected or ctl-MO-injected embryos), morphants (embryos injected with tM015b or sM015b morpholinos), and rescued embryos (embryos injected with tM015b and 50 pg of *smyhc1:col15a1b* construct). ***B***, Quantification of the escape response expressed as the time it takes for the embryo to reach out of the larger circle. ***C***, Quantification of the escape response is expressed as the mean of escape time ± SEM. Partial rescue of the motility phenotype is observed in 2 dpf embryos coinjected with tM015b and *smyhc1:col15a1b*. NS, Nonsignificant. *$p < 0.05$ (Student's *t* test). ***$p < 0.001$ (Student's *t* test).

network. COLXV-B colocalized with CS (Fig. 1*O*–*Q*). The identity of the CSPG present in the motor path is as yet unknown (Zhang et al., 2004). Collagen XV carries CS chains (Li et al., 2000), and it is possible that the reduction of CS staining in *unp* mutants (Zhang et al., 2004) is due to the reduction in COLXV-B deposition. These regulatory pathways are thus responsible for fine-tuning the COLXV-B spatio-temporal expression by slow muscle progenitors.

Several ECM cues involved in zebrafish axon pathfinding (CS, tenascin C, collagens XVIII and XIX) have been identified mainly through the combined analysis of gene expression patterns and mutants deficient in primary motor axon pathfinding, such as *diwanka/lh3* (Schneider and Granato, 2006), *unplugged/MuSK* (Zhang et al., 2004), and *stumpy/col19a1* (Hilario et al., 2010). However, except in the case of tenascin-C (Schweitzer et al., 2005), the presence of these molecular components in the motor path has not been shown. In this study, we have identified collagen XV-B as a bona fide component of the common motor path. Consistent with its specific localization in the motor path at the time of primary and secondary axon growth, we show that COLXV-B influences the decision of primary and secondary axons at the choice point. Primary and secondary motor axons share the same path, and it is likely that they will encounter the same positional cues on their route toward their target. Our data show that COLXV-B is instructive for the navigation of both motor axons. Interestingly, COLXV-B was much more critical for RoP-like and MiP-like axons to find their way. These data support previous findings that pathfinding rules are motoneuron-dependent. Indeed, cell-type sensitivity to guidance cues has already been reported for motor axons in zebrafish. Diwanka activity plays a differential role in ventral and dorsal nerve growth (Zeller et al., 2002), and both CaP and RoP primary and secondary motor axons, but not MiP ones, are dependent on *unplugged/MusK* (Zhang et al., 2001). The CaP axon was found to be sensitive to the extracellular molecule semaphorin 3A, but not MiP or RoP axons (Sato-Maeda et al., 2006), through the specific expression of the receptor neuro-

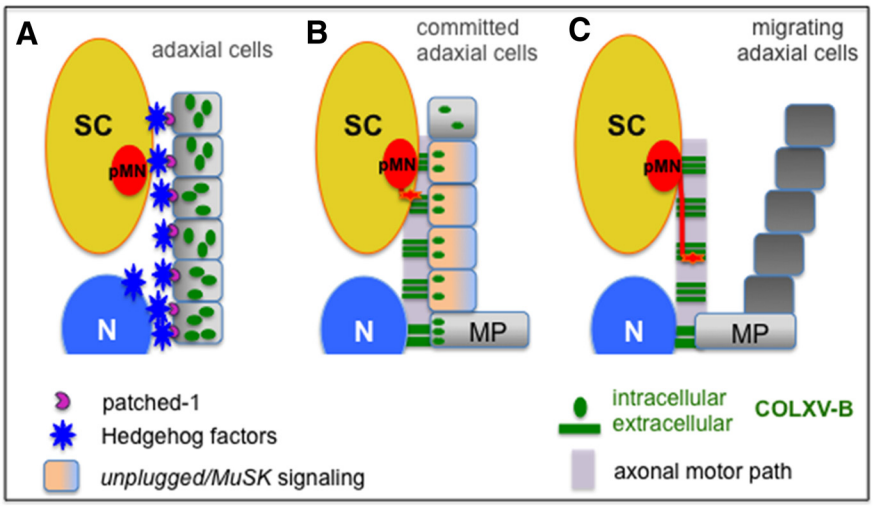

Figure 12. Model of the matrix COLXV-B fingerprint laid down by committed adaxial cells for motor axon navigation. ***A***, Expression of *col15a1b* in adaxial cells depends on Hh/Gli signaling. ***B***, COLXV-B protein is deposited and organized in the motor path upon *unplugged*/MuSK signaling. ***C***, COLXV-B is present in the motor path at the time of axon growth to provide a positional cue that guides axons toward intermediate targets.

pilin 1A and possibly the coreceptor plexin A3 (Feldner et al., 2005, 2007; Sato-Maeda et al., 2006).

The role of COLXV-B in axon pathfinding may rely on two plausible mechanisms. First, it has been suggested that COLXV-B interacts with ECM molecules to modulate their organization and function (Hurskainen et al., 2010). COLXV-B is thus a possible molecular candidate for orchestrating the organization of myotome-derived ECM molecules along the motor path. Second, COLXV-B may also function in axon pathfinding by interacting directly with a receptor expressed by growth cones, as was suggested for collagen XVIII, by binding to the membrane receptor RPTP (Schneider and Granato, 2006). Blocking the expression of neuropilin 1A and plexin A3 receptors resulted in additional exit points of axons from the spinal cord (Feldner et al., 2005, 2007; Palaisa and Granato, 2007). However, this defect was very rarely observed in the embryos overexpressing COLXV-B, suggesting that COLXV-B might not interact directly or indirectly with these receptors. Interestingly, the collagen-binding surface receptor DDR1 was found to guide axon along longitudinal tracts in *Caenorhabditis elegans* (Unsoeld et al., 2013). DDR1 directly interacts with the human protein COLXV in tumoral cells (Clementz et al., 2013). COLXV-B might interact with DDR1 to influence motor axon navigation.

Lack of COLXV-B also reduced embryo motility significantly in response to touch. Interestingly, the *unp/MuSK* mutant, which showed compromised COLXV-B deposition in the motor path, was also reported to exhibit decreased motility (Granato et al., 1996), but the cause is not clear. Muscle atrophy was observed in the absence of COLXV-B, which could explain the impaired swimming performance. Atrophy can result from reduced muscle excitation. Although synapses appeared to form normally in *col15a1b* morphants, defects in axon pathfinding can result in reduced innervation and motility defects. Consistent with this, a reduced number of neuromuscular synapses was associated with a significant reduction in myofibril content in a collection of mutants with defects in locomotor behavior (Panzer et al., 2005).

Despite its presence in skeletal muscle (Eklund et al., 2001) and motor nerve basement membranes (Rasi et al., 2010), very little is known about the function of collagen XV in the neuromuscular system. The analysis of *col15a1*$^{-/-}$ mice revealed that it functions as a structural component, required to stabilize skeletal muscle cells and blood vessels (Eklund et al., 2001), and that it also contributes to peripheral nerve maturation (Rasi et al., 2010). Here we provide the first evidence that zebrafish COLXV-B functions as a motor axon pathfinder. A role in axonal guidance was demonstrated for the collagen XV/XVIII homolog CLE-1 in *C. elegans* (Ackley et al., 2001) and for the multiplexin Mp in flies (Meyer and Moussian, 2009), suggesting a conserved role for multiplexins during evolution. No human disease has so far been associated with mutations in the *COL15A1* gene. Most molecular cues and signaling pathways in the neuromuscular system are common to humans and zebrafish, suggesting that *COL15A1* might represent a candidate gene for orphan neuromuscular disorders, as previously suggested (Rasi et al., 2010).

References

Ackley BD, Crew JR, Elamaa H, Pihlajaniemi T, Kuo CJ, Kramer JM (2001) The NC1/endostatin domain of *Caenorhabditis elegans* type XVIII collagen affects cell migration and axon guidance. J Cell Biol 152:1219–1232. CrossRef Medline

Bader HL, Keene DR, Charvet B, Veit G, Driever W, Koch M, Ruggiero F (2009) Zebrafish collagen XII is present in embryonic connective tissue sheaths (fascia) and basement membranes. Matrix Biol 28:32–43. CrossRef Medline

Beattie CE (2000) Control of motor axon guidance in the zebrafish embryo. Brain Res Bull 53:489–500. CrossRef Medline

Bernhardt RR, Schachner M (2000) Chondroitin sulfates affect the formation of the segmental motor nerves in zebrafish embryos. Dev Biol 221:206–219. CrossRef Medline

Bretaud S, Pagnon-Minot A, Guillon E, Ruggiero F, Le Guellec D (2011) Characterization of spatial and temporal expression pattern of Col15a1b during zebrafish development. Gene Expr Patterns 11:129–134. CrossRef Medline

Clementz AG, Mutolo MJ, Leir SH, Morris KJ, Kucybala K, Harris H, Harris A (2013) Collagen XV inhibits epithelial to mesenchymal transition in pancreatic adenocarcinoma cells. PLoS One 8:e72250. CrossRef Medline

Concordet JP, Lewis KE, Moore JW, Goodrich LV, Johnson RL, Scott MP, Ingham PW (1996) Spatial regulation of a zebrafish patched homologue reflects the roles of sonic hedgehog and protein kinase A in neural tube and somite patterning. Development 122:2835–2846. Medline

Daggett DF, Domingo CR, Currie PD, Amacher SL (2007) Control of morphogenetic cell movements in the early zebrafish myotome. Dev Biol 309:169–179. CrossRef Medline

Du SJ, Devoto SH, Westerfield M, Moon RT (1997) Positive and negative regulation of muscle cell identity by members of the hedgehog and TGF-β gene families. J Cell Biol 139:145–156. CrossRef Medline

Eisen JS, Pike SH (1991) The spt-1 mutation alters segmental arrangement and axonal development of identified neurons in the spinal cord of the embryonic zebrafish. Neuron 6:767–776. CrossRef Medline

Ekker M, Wegner J, Akimenko MA, Westerfield M (1992) Coordinate embryonic expression of three zebrafish engrailed genes. Development 116:1001–1010. Medline

Eklund L, Muona A, Liétard J, Pihlajaniemi T (2000) Structure of the mouse type XV collagen gene, Col15a1: comparison with the human COL15A1 gene and functional analysis of the promoters of both genes. Matrix Biol 19:489–500. CrossRef Medline

Eklund L, Piuhola J, Komulainen J, Sormunen R, Ongvarrasopone C, Fässler R, Muona A, Ilves M, Ruskoaho H, Takala TE, Pihlajaniemi T (2001) Lack of type XV collagen causes a skeletal myopathy and cardiovascular defects in mice. Proc Natl Acad Sci U S A 98:1194–1199. CrossRef Medline

Elworthy S, Hargrave M, Knight R, Mebus K, Ingham PW (2008) Expression of multiple slow myosin heavy chain genes reveals a diversity of zebrafish slow twitch muscle fibres with differing requirements for Hedgehog and Prdm1 activity. Development 135:2115–2126. CrossRef Medline

Feldner J, Becker T, Goishi K, Schweitzer J, Lee P, Schachner M, Klagsbrun M, Becker CG (2005) Neuropilin-1a is involved in trunk motor axon outgrowth in embryonic zebrafish. Dev Dyn 234:535–549. CrossRef Medline

Feldner J, Reimer MM, Schweitzer J, Wendik B, Meyer D, Becker T, Becker CG (2007) PlexinA3 restricts spinal exit points and branching of trunk motor nerves in embryonic zebrafish. J Neurosci 27:4978–4983. CrossRef Medline

Fox MA (2008) Novel roles for collagens in wiring the vertebrate nervous system. Curr Opin Cell Biol 20:508–513. CrossRef Medline

Gerety SS, Wilkinson DG (2011) Morpholino artifacts provide pitfalls and reveal a novel role for pro-apoptotic genes in hindbrain boundary development. Dev Biol 350:279–289. CrossRef Medline

Goody MF, Kelly MW, Reynolds CJ, Khalil A, Crawford BD, Henry CA (2012) NAD$^+$ biosynthesis ameliorates a zebrafish model of muscular dystrophy. PLoS Biol 10:e1001409. CrossRef Medline

Granato M, van Eeden FJ, Schach U, Trowe T, Brand M, Furutani-Seiki M, Haffter P, Hammerschmidt M, Heisenberg CP, Jiang YJ, Kane DA, Kelsh RN, Mullins MC, Odenthal J, Nüsslein-Volhard C (1996) Genes controlling and mediating locomotion behavior of the zebrafish embryo and larva. Development 123:399–413. Medline

Haftek Z, Morvan-Dubois G, Thisse B, Thisse C, Garrone R, Le Guellec D (2003) Sequence and embryonic expression of collagen XVIII NC1 domain (endostatin) in the zebrafish. Gene Expr Patterns 3:351–354. CrossRef Medline

Hilario JD, Wang C, Beattie CE (2010) Collagen XIXa1 is crucial for motor axon navigation at intermediate targets. Development 137:4261–4269. CrossRef Medline

Hurskainen M, Ruggiero F, Hägg P, Pihlajaniemi T, Huhtala P (2010) Recombinant human collagen XV regulates cell adhesion and migration. J Biol Chem 285:5258–5265. CrossRef Medline

Jackson HE, Ingham PW (2013) Control of muscle fibre-type diversity during embryonic development: the zebrafish paradigm. Mech Dev 130: 447–457. CrossRef Medline

Kimmel CB, Ballard WW, Kimmel SR, Ullmann B, Schilling TF (1995) Stages of embryonic development of the zebrafish. Dev Dyn 203:253–310. CrossRef Medline

Koudijs MJ, den Broeder MJ, Groot E, van Eeden FJ (2008) Genetic analysis of the two zebrafish patched homologues identifies novel roles for the hedgehog signaling pathway. BMC Dev Biol 8:15. CrossRef Medline

Li D, Clark CC, Myers JC (2000) Basement membrane zone type XV collagen is a disulfide-bonded chondroitin sulfate proteoglycan in human tissues and cultured cells. J Biol Chem 275:22339–22347. CrossRef Medline

Matys V, Kel-Margoulis OV, Fricke E, Liebich I, Land S, Barre-Dirrie A, Reuter I, Chekmenev D, Krull M, Hornischer K, Voss N, Stegmaier P, Lewicki-Potapov B, Saxel H, Kel AE, Wingender E (2006) TRANSFAC and its module TRANSCompel: transcriptional gene regulation in eukaryotes. Nucleic Acids Res 34(Database issue):D108–D110. CrossRef Medline

Melançon E, Liu DW, Westerfield M, Eisen JS (1997) Pathfinding by identified zebrafish motoneurons in the absence of muscle pioneers. J Neurosci 17:7796–7804. Medline

Meyer F, Moussian B (2009) *Drosophila* multiplexin (Dmp) modulates motor axon pathfinding accuracy. Dev Growth Differ 51:483–498. CrossRef Medline

Milla LA, Cortés CR, Hodar C, Oñate MG, Cambiazo V, Burgess SM, Palma V (2012) Yeast-based assay identifies novel Shh/Gli target genes in vertebrate development. BMC Genomics 13:2. CrossRef Medline

Nguyen-Chi ME, Bryson-Richardson R, Sonntag C, Hall TE, Gibson A, Sztal T, Chua W, Schilling TF, Currie PD (2012) Morphogenesis and cell fate determination within the adaxial cell equivalence group of the zebrafish myotome. PLoS Genet 8:e1003014. CrossRef Medline

Pagnon-Minot A, Malbouyres M, Haftek-Terreau Z, Kim HR, Sasaki T, Thisse C, Thisse B, Ingham PW, Ruggiero F, Le Guellec D (2008) Collagen XV, a novel factor in zebrafish notochord differentiation and muscle development. Dev Biol 316:21–35. CrossRef Medline

Palaisa KA, Granato M (2007) Analysis of zebrafish sidetracked mutants reveals a novel role for Plexin A3 in intraspinal motor axon guidance. Development 134:3251–3257. CrossRef Medline

Panzer JA, Gibbs SM, Dosch R, Wagner D, Mullins MC, Granato M, Balice-Gordon RJ (2005) Neuromuscular synaptogenesis in wild-type and mutant zebrafish. Dev Biol 285:340–357. CrossRef Medline

Rasi K, Hurskainen M, Kallio M, Stavén S, Sormunen R, Heape AM, Avila RL, Kirschner D, Muona A, Tolonen U, Tanila H, Huhtala P, Soininen R, Pihlajaniemi T (2010) Lack of collagen XV impairs peripheral nerve maturation and, when combined with laminin-411 deficiency, leads to basement membrane abnormalities and sensorimotor dysfunction. J Neurosci 30:14490–14501. CrossRef Medline

Ricard-Blum S, Ruggiero F (2005) The collagen superfamily: from the extracellular matrix to the cell membrane. Pathol Biol 53:430–442. CrossRef Medline

Robu ME, Larson JD, Nasevicius A, Beiraghi S, Brenner C, Farber SA, Ekker SC (2007) p53 activation by knockdown technologies. PLoS Genet 3:e78. CrossRef Medline

Sato-Maeda M, Tawarayama H, Obinata M, Kuwada JY, Shoji W (2006) Sema3a1 guides spinal motor axons in a cell- and stage-specific manner in zebrafish. Development 133:937–947. CrossRef Medline

Schneider VA, Granato M (2006) The myotomal diwanka (lh3) glycosyltransferase and type XVIII collagen are critical for motor growth cone migration. Neuron 50:683–695. CrossRef Medline

Schweitzer J, Becker T, Lefebvre J, Granato M, Schachner M, Becker CG (2005) Tenascin-C is involved in motor axon outgrowth in the trunk of developing zebrafish. Dev Dyn 234:550–566. CrossRef Medline

Soroldoni D, Hogan BM, Oates AC (2009) Simple and efficient transgenesis with meganuclease constructs in zebrafish. Methods Mol Biol 546: 117–130. CrossRef Medline

Takeuchi M, Kaneko H, Nishikawa K, Kawakami K, Yamamoto M, Kobayashi M (2010) Efficient transient rescue of hematopoietic mutant phenotypes in zebrafish using Tol2-mediated transgenesis. Dev Growth Differ 52:245–250. CrossRef Medline

Thomas-Chollier M, Defrance M, Medina-Rivera A, Sand O, Herrmann C, Thieffry D, van Helden J (2011) RSAT 2011: regulatory sequence analysis tools. Nucleic Acids Res 39 (Web Server issue):W86–W91. CrossRef Medline

Unsoeld T, Park JO, Hutter H (2013) Discoidin domain receptors guide axons along longitudinal tracts in *C. elegans*. Dev Biol 374:142–152. CrossRef Medline

Zeller J, Schneider V, Malayaman S, Higashijima S, Okamoto H, Gui J, Lin S, Granato M (2002) Migration of zebrafish spinal motor nerves into the periphery requires multiple myotome-derived cues. Dev Biol 252: 241–256. CrossRef Medline

Zhang J, Granato M (2000) The zebrafish unplugged gene controls motor axon pathway selection. Development 127:2099–2111. Medline

Zhang J, Malayaman S, Davis C, Granato M (2001) A dual role for the zebrafish unplugged gene in motor axon pathfinding and pharyngeal development. Dev Biol 240:560–573. CrossRef Medline

Zhang J, Lefebvre JL, Zhao S, Granato M (2004) Zebrafish unplugged reveals a role for muscle-specific kinase homologs in axonal pathway choice. Nat Neurosci 7:1303–1309. CrossRef Medline